Constitutive Relations and Parameter Estimation for Finite Deformations of Viscoelastic Adhesives

G. O. Antoine
Department of Biomedical Engineering and Mechanics (M/C 0219),
Virginia Polytechnic Institute and State University,
Blacksburg, VA 24061
e-mail: antoineg@vt.edu

R. C. Batra[1]
Fellow ASME
Department of Biomedical Engineering and Mechanics (M/C 0219),
Virginia Polytechnic Institute and State University,
Blacksburg, VA 24061
e-mail: rbatra@vt.edu

We propose a constitutive relation for finite deformations of nearly incompressible isotropic viscoelastic rubbery adhesives assuming that the Cauchy stress tensor can be written as the sum of elastic and viscoelastic parts. The former is derived from a stored energy function and the latter from a hereditary type integral. Using Ogden's expression for the strain energy density and the Prony series for the viscoelastic shear modulus, values of material parameters are estimated by using experimental data for uniaxial tensile and compressive cyclic deformations at different constant engineering axial strain rates. It is found that values of material parameters using the loading part of the first cycle, the complete first cycle, and the complete two loading cycles are quite different. Furthermore, the constitutive relation with values of material parameters determined from the monotonic loading during the first cycle of deformations cannot well predict even deformations during the unloading portion of the first cycle. The developed constitutive relation is used to study low-velocity impact of polymethylmethacrylate (PMMA)/adhesive/polycarbonate (PC) laminate. The three sets of values of material parameters for the adhesive seem to have a negligible effect on the overall deformations of the laminate. It is attributed to the fact that peak strain rates in the severely deforming regions are large, and the corresponding stresses are essentially unaffected by the long time response of the adhesive. [DOI: 10.1115/1.4029057]

Keywords: viscoelasticity, finite deformations, constitutive equations, parameter estimation, low-velocity impact

Introduction

Thermoplastic polyurethanes (TPUs) are a class of polymers composed of soft and hard segments which form a two-phase microstructure (e.g., see Refs. [1–4]). The soft segments account for the high extension and elastic recovery, while the hard segments provide high modulus and strength [5]. The TPUs often exhibit a strain-rate and temperature dependent response to mechanical deformations. The viscous response is related to relative sliding of a molecule with respect to its neighbors [6]. It is quite challenging to model the large strain viscoelastic response of the TPUs.

The high elasticity, flexibility, resistance to abrasion and impact, and the ease in processing TPUs have significantly increased their applications in diverse areas. Their use as bonding interlayers in structures subjected to impact and blast loading is believed to increase the survivability of structures. In particular, Tasdemirci et al. [7] have shown that the choice of an adhesive interlayer influences the damage induced in a structure subjected to impact. They used a split Hopkinson pressure bar and numerical simulations to study the response of an alumina ceramic/adhesive/glass-epoxy laminate to an incident compressive stress wave. Considering the damage induced in the glass-epoxy plate as the critical parameter for impact resistance, they concluded that the low acoustic impedance of the bonding interlayer reduced the damage induced in the back plate, since it transmits less stress from the front layer to the back plate. We note that constituents of a structure subjected to impact loads usually undergo large strains and varying strain rates. Thus, the study of the response of TPUs for large strains and over a wide range of strain-rates (e.g., 10^{-3} to 10^3/s) is fundamental to understanding the dynamic response of structures using TPUs and is of great engineering relevance.

Kihara et al. [8] experimentally measured the impact shear strength of an electroconductive material and an epoxy resin and performed finite element (FE) simulations to determine the maximum shear stress in the sample at fracture. They concluded that the maximum shear stress equals the impact shear strength of the adhesive. Boyce et al. [4] experimentally found that the representative PUs considered in their study transitioned from rubberylike behavior at strain rate of 10^{-3} to leathery/glassylike behavior at strain rates of 10^3/s. Similar results were obtained by Sarva et al. [9] who investigated the response of a polyurea and a polyurethane ("PU2") for compressive strain rates between 10^{-3} and 10^4/s. They found that at room temperature the behavior of the PU2 transitioned from rubbery at strain rates of $\sim$0.002/s to leathery at 0.1/s and to glassy at strain rates $>10^3$/s.

Numerical simulations are being increasingly used to replace physical experiments, since they reduce time, cost, and materials. They also provide details of deformations in the interior of a structure not easily accessible through experimental measurements. This requires reliable constitutive equations for all materials used in a structure including the TPUs. Challenges in modeling the response of TPUs include large deformations, strain-rate, and temperature-dependence of their response. The elastic response of incompressible hyperelastic rubbers has been investigated by Rivlin and Saunders [10], Ericksen [11], and Ogden [12] amongst others. The Mooney–Rivlin material model and the empirical strain-energy density function proposed by Ogden [12] have been implemented in many commercial softwares. Arruda and Boyce [13] proposed an eight-chain network model in which the material is assumed to be an assembly of cubic material particles, each containing eight chains originating from the cube centroid and

[1]Corresponding author.

Manuscript received July 17, 2014; final manuscript received November 9, 2014; accepted manuscript posted November 13, 2014; published online December 11, 2014. Assoc. Editor: Weinong Chen.

ending at its vertices. Using Langevin's work on chains, they developed a temperature-dependent strain energy density potential with a small number of material parameters. Coleman and Noll [14] employed concepts of materials with fading memory and developed a hereditary type constitutive relation for finite deformations of viscoelastic materials. Christensen [15] expressed these constitutive relations as convolution integrals involving a relaxation moduli and the time rate of the Green–St. Venant strain tensor and showed that the relaxation moduli can be determined with a set of simple tests (simple shear, creep). Qi and Boyce [16] relying on the works of Boyce et al. [17,18] assumed that the response of a TPU is the sum of a nonlinear elastic contribution modeled with a Langevin spring and a viscoelastoplastic stress (nonlinear spring–dashpot system) capturing the rate-dependent response of the material with both contributions being temperature dependent. They showed that this model predicts well the response of a TPU specimen under tensile and compressive cyclic loadings at strain rates from 0.01/s to 0.1/s.

A challenging and somewhat unresolved issue is that of finding values of material parameters and what portion of the test data to use. This is compounded by the observation that most experiments are conducted at constant nominal strain rates, whereas the material response depends upon the current or the true strain rate. Here, we assume that the viscoelastic response of a TPU can be modeled as the sum of two terms—elastic represented by Ogden's form of the strain energy density function and viscous represented by a hereditary type integral of the type employed by Christensen. Of course, the hereditary type integral also includes the instantaneous elastic response of the material. We then use the uniaxial deformations test data at constant engineering axial strain rate for the first loading, the first complete cycle of loading and unloading, and the first two loading and unloading cycles to find values of material parameters appearing in the assumed constitutive relation. The time delay between the two cycles is also considered. The number of material parameters in the constitutive relation needed to reasonably well replicate the experimental uniaxial stress–uniaxial strain curves varies with the amount of test data employed. This constitutive relation has been implemented in the commercial software, LSDYNA, and used to study the low-velocity impact response of a PMMA/adhesive/PC laminate which is similar to the work of Antoine and Batra [19].

Constitutive Relations

We assume that a TPU can be modeled as an isotropic, viscoelastic, and nearly incompressible material. A one-dimensional mechanical analog of the material model described in this section is shown in Fig. 1.

The total response of the material consists of a nonlinear spring ($\boldsymbol{\sigma}^{\rm nlel}$) accounting for the quasi-static (very low strain rate) elastic response of the material and the viscoelastic response ($\boldsymbol{\sigma}^{\rm ve}$) modeled with a Maxwell ladder (Prony series). The kinematic constraint of incompressibility of the material requires an additional contribution in the form of a pressure term where the pressure p is a Lagrange multiplier and cannot be found from deformations of the material but is determined by solving an initial-boundary-value problem in which normal tractions must be prescribed on a part of the boundary of the body. Thus, the total Cauchy stress $\boldsymbol{\sigma}$ at a material point is expressed as

$$\boldsymbol{\sigma} = \boldsymbol{\sigma}^{\rm nlel} + \boldsymbol{\sigma}^{\rm ve} - p\mathbf{I} \tag{1}$$

where $\mathbf{I}$ is the identity tensor.

We assume that the material is hyperelastic. For the strain energy density potential W, we use the following form proposed by Ogden [20]:

$$W = \sum_{n=1}^{N} \frac{\mu_n}{\alpha_n}\left(\lambda_1^{\alpha_n} + \lambda_2^{\alpha_n} + \lambda_3^{\alpha_n} - 3\right) \tag{2}$$

In Eq. (2), N is an integer, $\{\mu_n\}_{n=1,\ldots,N}$ and $\{\alpha_n\}_{n=1,\ldots,N}$ are material parameters, and $\{\lambda_i\}_{i=1,2,3}$ are principal stretches satisfying the incompressibility constraint $\lambda_1\lambda_2\lambda_3 = 1$.

In order to motivate the choice of the constitutive equation for the viscoelastic response of the material, we consider a one-dimensional linear Maxwell model sketched in Fig. 2. Thus,

$$\begin{cases} \sigma = \sigma_k = \sigma_\eta, & \varepsilon = \varepsilon_k + \varepsilon_\eta \\ \sigma_\eta = \eta\dot{\varepsilon}_\eta, & \sigma_k = k\varepsilon_k \end{cases} \tag{3}$$

where k is the spring constant, σ is the axial stress, ε is the axial strain, η is the viscosity, and a superimposed dot indicates the material time derivative. Equations (3) give

$$\dot{\sigma} = k\dot{\varepsilon} - \frac{k}{\eta}\sigma \tag{4}$$

Motivated by Eq. (4), the viscoelastic response $\boldsymbol{\sigma}^{\rm ve}$ of the material for three-dimensional deformations is modeled with the following Prony series:

$$\boldsymbol{\sigma}^{\rm ve} = \sum_{m=1}^{M} \boldsymbol{\sigma}_m^{\rm ve}, \quad \begin{cases} \overset{\bullet}{\boldsymbol{\sigma}}{}_m^{\rm ve} = 2G_m\mathbf{D} - \beta_m\boldsymbol{\sigma}_m^{\rm ve} \\ \boldsymbol{\sigma}_m^{\rm ve}|_{t=0} = 0 \end{cases} \tag{5}$$

In Eq. (5), $\overset{\bullet}{\boldsymbol{\sigma}}{}_m^{\rm ve}$ is the Green and Naghdi [21] objective rate-of-stress tensor, $\mathbf{D}$ is the deviatoric part of the strain-rate tensor, G_m and β_m are material parameters that can be thought of as shear moduli and decay constants, respectively, and M is an integer. We note that Eq. (5) accounts for geometric nonlinearities, is materially objective, is valid for finite deformations, and $\mathbf{D}$ does not equal the time rate of a strain tensor unless the present configuration is taken as the reference configuration, e.g., see Ref. [22].

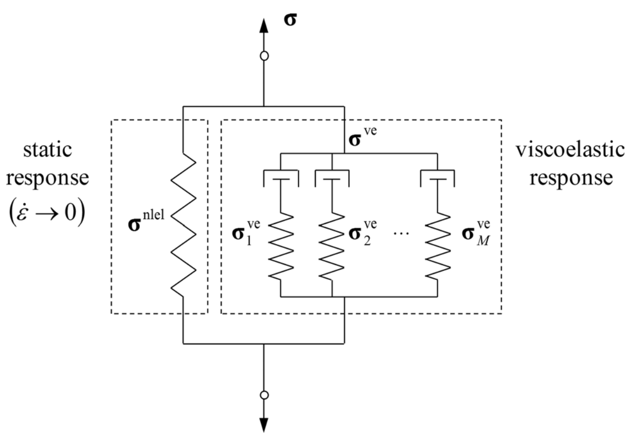

Fig. 1 One-dimensional rheological analog interpretation of the material model

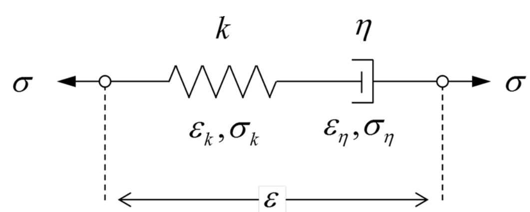

Fig. 2 One-dimensional Maxwell model

The energy dissipated per unit volume, $E^{\mathrm{visc,ve}}$, during finite deformations of the material obeying Eq. (5) is given by

$$E^{\mathrm{visc,ve}} = \int_t \left[\sum_{m=1}^{M} \left(\frac{\beta_m}{2G_m} \boldsymbol{\sigma}_m^{\mathrm{ve}} : \boldsymbol{\sigma}_m^{\mathrm{ve}} \right) dt \right] \tag{6}$$

where $\boldsymbol{\sigma}_m^{\mathrm{ve}} : \boldsymbol{\sigma}_m^{\mathrm{ve}}$ denotes inner product of second order tensors $\boldsymbol{\sigma}_m^{\mathrm{ve}}$ and $\boldsymbol{\sigma}_m^{\mathrm{ve}}$. Equation (6) is derived in the Appendix.

Values of the Material Parameters

Analytical Expression for the Axial Stress for Uniaxial Tensile and Compressive Deformations at Constant Engineering Strain Rate. Of special interest here are cyclic uniaxial tension or compression tests since viscoelastic materials exhibit hysteresis, and the area between the loading and the unloading curves is related to the energy dissipated due to viscous deformations of the material. These tests are displacement-controlled and are often performed at constant engineering strain rate by clamping one end of the sample and prescribing a constant velocity at the other end. For finite deformations, the difference between the engineering strain rate and the true strain rate cannot be neglected. Accordingly, we present relations giving the axial Cauchy stress (or true stress) as a function of the axial stretch and the engineering axial strain rate for the first and the second loading–unloading cycles of a cyclic test performed at a constant engineering strain rate for a material obeying the constitutive relations (1) with W and $\boldsymbol{\sigma}^{\mathrm{ve}}$ given by Eqs. (2) and (5), respectively. The derivation of these expressions is given in the Appendix where expressions for the third and the fourth loading–unloading cycles are also given.

We use the following notation: σ^{True} is the true axial stress, λ is the axial stretch, $\dot{\varepsilon}^{\mathrm{Eng}}$ is the constant engineering strain rate (taken positive for both loading and unloading), $\lambda_{\mathrm{I}}^{\mathrm{p}}$ and $\lambda_{\mathrm{II}}^{\mathrm{p}}$ are the maximum axial stretch of the first and the second cycles, respectively, and Δt is the delay time between the end of the first cycle and the beginning of the second cycle. We introduce functions $\mathrm{I}_{\mathrm{load}}(\dot{\varepsilon}^{\mathrm{Eng}}, G, \beta, \lambda)$ and $\mathrm{I}_{\mathrm{unload}}(\dot{\varepsilon}^{\mathrm{Eng}}, G, \beta, \lambda_0, \lambda)$ defined as

$$I_{\mathrm{load}}\left(\dot{\varepsilon}^{\mathrm{Eng}}, G, \beta, \lambda\right) = 3G \exp\left(-\frac{\beta\lambda}{\dot{\varepsilon}^{\mathrm{Eng}}}\right)\left[\mathrm{Ei}\left(\frac{\beta\lambda}{\dot{\varepsilon}^{\mathrm{Eng}}}\right) - \mathrm{Ei}\left(\frac{\beta}{\dot{\varepsilon}^{\mathrm{Eng}}}\right)\right] \tag{7a}$$

$$I_{\mathrm{unload}}\left(\dot{\varepsilon}^{\mathrm{Eng}}, G, \beta, \lambda_0, \lambda\right) = 3G \exp\left(\frac{\beta\lambda}{\dot{\varepsilon}^{\mathrm{Eng}}}\right)\left[\mathrm{Ei}\left(-\frac{\beta\lambda}{\dot{\varepsilon}^{\mathrm{Eng}}}\right) - \mathrm{Ei}\left(\frac{\beta\lambda_0}{\dot{\varepsilon}^{\mathrm{Eng}}}\right)\right] \tag{7b}$$

where $\mathrm{Ei}(x) = -\int_{\xi=-x}^{+\infty}((e^{-\xi}/\xi)d\xi)$ and the integral is understood as the Cauchy principal value due to the singularity of the integrand at $\xi = 0$.

For an incompressible material, expressions giving the true axial stress as a function of the axial stretch and the engineering strain rate without explicit reference to time are listed below:

- First cycle, loading:

$$\begin{aligned}\sigma_{\mathrm{I,load}}^{\mathrm{True}}(\lambda) &= \sum_{n=1}^{N} \mu_n\left(\lambda^{\alpha_n} - \lambda^{-\alpha_n/2}\right)\\ &\quad + \sum_{m=1}^{M} 3G_m \exp\left(-\frac{\beta_m\lambda}{\dot{\varepsilon}^{\mathrm{Eng}}}\right)\left[\mathrm{Ei}\left(\frac{\beta_m\lambda}{\dot{\varepsilon}^{\mathrm{Eng}}}\right) - \mathrm{Ei}\left(\frac{\beta_m}{\dot{\varepsilon}^{\mathrm{Eng}}}\right)\right]\end{aligned} \tag{8}$$

- First cycle, unloading:

$$\begin{aligned}\sigma_{\mathrm{I,unload}}^{\mathrm{True}}(\lambda) &= \sum_{n=1}^{N} \mu_n\left(\lambda^{\alpha_n} - \lambda^{-\alpha_n/2}\right)\\ &\quad + \sum_{m=1}^{M} 3G_m \exp\left(-\beta_m \frac{2\lambda_{\mathrm{I}}^{\mathrm{p}} - \lambda}{\dot{\varepsilon}^{\mathrm{Eng}}}\right)\left[\mathrm{Ei}\left(\frac{\beta_m\lambda_{\mathrm{I}}^{\mathrm{p}}}{\dot{\varepsilon}^{\mathrm{Eng}}}\right)\right.\\ &\quad \left. - \mathrm{Ei}\left(\frac{\beta_m}{\dot{\varepsilon}^{\mathrm{Eng}}}\right)\right] + \sum_{m=1}^{M} 3G_m \exp\left(\frac{\beta_m\lambda}{\dot{\varepsilon}^{\mathrm{Eng}}}\right)\\ &\quad \times \left[\mathrm{Ei}\left(-\frac{\beta_m\lambda}{\dot{\varepsilon}^{\mathrm{Eng}}}\right) - \mathrm{Ei}\left(\frac{\beta_m\lambda_{\mathrm{I}}^{\mathrm{p}}}{\dot{\varepsilon}^{\mathrm{Eng}}}\right)\right]\end{aligned} \tag{9}$$

- Second cycle, loading:

$$\begin{aligned}\sigma_{II,\mathrm{unload}}^{\mathrm{True}}(\lambda) &= \sum_{n=1}^{N} \mu_n\left(\lambda^{\alpha_n} - \lambda^{-\alpha_n/2}\right)\\ &\quad + \sum_{m=1}^{M} \exp\left(-\beta_m\left(\Delta t + \frac{\lambda + \lambda_{\mathrm{I}}^{\mathrm{p}} - 2}{\dot{\varepsilon}^{\mathrm{Eng}}}\right)\right)\\ &\quad \times \mathrm{I}_{\mathrm{load}}\left(\dot{\varepsilon}^{\mathrm{Eng}}, G_m, \beta_m, \lambda_{\mathrm{I}}^{\mathrm{p}}\right)\\ &\quad + \sum_{m=1}^{M} \exp\left(-\beta_m\left(\Delta t + \frac{\lambda - 1}{\dot{\varepsilon}^{\mathrm{Eng}}}\right)\right)\\ &\quad \times \mathrm{I}_{\mathrm{unload}}\left(\dot{\varepsilon}^{\mathrm{Eng}}, G_m, \beta_m, \lambda_{\mathrm{I}}^{\mathrm{p}}, 1\right)\\ &\quad + \sum_{m=1}^{M} \mathrm{I}_{\mathrm{load}}\left(\dot{\varepsilon}^{\mathrm{Eng}}, G_m, \beta_m, \lambda\right)\end{aligned} \tag{10}$$

- Second cycle, unloading:

$$\begin{aligned}\sigma_{II,\mathrm{unload}}^{\mathrm{True}}(\lambda) &= \sum_{n=1}^{N} \mu_n\left(\lambda^{\alpha_n} - \lambda^{-\alpha_n/2}\right)\\ &\quad + \sum_{m=1}^{M} \exp\left(-\beta_m\left(\Delta t + \frac{\lambda_{\mathrm{I}}^{\mathrm{p}} + 2\lambda_{\mathrm{II}}^{\mathrm{p}} - 2 - \lambda}{\dot{\varepsilon}^{\mathrm{Eng}}}\right)\right)\\ &\quad \times \mathrm{I}_{\mathrm{load}}\left(\dot{\varepsilon}^{\mathrm{Eng}}, G_m, \beta_m, \lambda_{L}^{\mathrm{p}}\right)\\ &\quad + \sum_{m=1}^{M} \exp\left(-\beta_m\left(\Delta t + \frac{2\lambda_{\mathrm{II}}^{\mathrm{p}} - 1 - \lambda}{\dot{\varepsilon}^{\mathrm{Eng}}}\right)\right)\\ &\quad \times \mathrm{I}_{\mathrm{unload}}\left(\dot{\varepsilon}^{\mathrm{Eng}}, G_m, \beta_m, \lambda_{\mathrm{I}}^{\mathrm{p}}, 1\right)\\ &\quad + \sum_{m=1}^{M} \exp\left(-\beta_m \frac{\lambda_{\mathrm{II}}^{\mathrm{p}} - \lambda}{\dot{\varepsilon}^{\mathrm{Eng}}}\right)\mathrm{I}_{\mathrm{load}}\left(\dot{\varepsilon}^{\mathrm{Eng}}, G_m, \beta_m, \lambda_{\mathrm{II}}^{\mathrm{p}}\right)\\ &\quad + \sum_{m=1}^{M} \mathrm{I}_{\mathrm{unload}}\left(\dot{\varepsilon}^{\mathrm{Eng}}, G_m, \beta_m, \lambda_{\mathrm{II}}^{\mathrm{p}}, \lambda\right)\end{aligned} \tag{11}$$

For monotonic uniaxial compression, the axial stress can be found from Eq. (8) by substituting a negative value for the constant engineering strain rate.

Materials and Experimental Data. The two model adhesives considered in this work are the transparent TPUs DFA4700 (Dureflex® A4700) and IM800A (INTER Materials 800A). Stenzler [23] has provided test data for these two materials for uniaxial tests summarized in Table 1. For the cyclic tensile tests, the materials were deformed up to a prescribed strain, then unloaded to zero strain, and allowed to relax for $\Delta t = 30$ s between the cycles.

Table 1 Test conditions for data available for DFA4700 and IM800A [23]

Type of test	Strain rate $\dot{\varepsilon}^{\mathrm{Eng}}$ (/s)	Number of cycles	Amplitude
Monotonic compression	−0.001	/	$\varepsilon_{\mathrm{min}}^{\mathrm{Eng}} = -0.2$
Monotonic tension	5.0	/	$\varepsilon_{\mathrm{max}}^{\mathrm{Eng}} = 1$
Cyclic tension	0.01, 0.1, 0.5	4	$\varepsilon_{\mathrm{max}}^{\mathrm{Eng}} = 1, 2, 3, 4$
Cyclic tension	1.0	1	$\varepsilon_{\mathrm{max}}^{\mathrm{Eng}} = 1$

The peak engineering strains of the cyclic tests were gradually increased from 1 for the first cycle to 4 for the fourth cycle.

Method and Results. The material parameters to be determined are the number N of terms in the Ogden potential and the corresponding parameters $\{\mu_n\}_{1\le n\le N}$ and $\{\alpha_n\}_{1\le n\le N}$, and the number M of terms in the Prony series and the corresponding shear moduli $\{G_m\}_{1\le m\le M}$ and decay constants $\{\beta_m\}_{1\le m\le M}$. Values of N and M are progressively increased until the deviation in the L^2-norm between the experimental stress–strain curve considered and the corresponding model prediction (Eqs. (8)–(11)) is less than 15%. The procedure is applied three times for successively larger test data.

For case 1, we only consider the monotonic compression (−0.001/s) and tension (5/s) tests and the loading portion of the first cycle of the cyclic tensile tests at all strain rates (0.01/s, 0.1/s, 0.5/s, and 1.0/s). For case 2, we consider the complete first cycle of the cyclic tests in addition to the data included for case 1. For case 3, we consider the data for the first two complete cycles.

The optimal set of parameters is searched using MATHEMATICA and the “FindFit” function. The functions listed in Eqs. (8)–(11) are written for assumed values of N and M and a least-square fit of the stress predictions with the corresponding experimental curves is performed. The values of N and M are gradually increased till the L^2-norm of the deviation is less than 15%. When the third cycle was included in the fitting no value of N and M could be found to achieve the desired deviation. Accordingly, we discuss results obtained with only two cycles of loading/unloading. Moreover, no acceptable fit could be found for the DFA4700 when the second cycle was included. Deviations of about 25% are persistent despite increasing values of N and M. We will present here the results obtained for $N=1$ and $M=5$. Using stress, strain, and strain-rate relations other than those given by Eqs. (8)–(11) was not investigated.

Values of material parameters for cases 1, 2, and 3 found using the above-mentioned procedure are listed in Table 2 for the DFA4700 and the IM800A.

The percentage deviations between the experimental data and the model prediction are given in Table 3. For cases 1 and 2, the deviations between the model predictions and the experimental results not included in the least-square fit are large. In particular, more than 200% deviation is observed for DFA4700 between predictions of the second tensile cycle and the results of case 2 while smaller deviations are obtained with case 1. Thus, one cannot hope to correctly predict the experimental data not included in finding optimal values of the material parameters, and that improving the agreement with the first complete deformation

Table 2 Values of material parameters for the DFA4700 and the IM800A TPUs

	Experimental data considered for the three cases					
Experimental data considered	Case 1		Case 2		Case 3	
Compression	✓		✓		✓	
Cycle 1, loading	✓		✓		✓	
Cycle 1, unloading	×		✓		✓	
Cycle 2	×		×		✓	
	Optimal values of the material parameters for the DFA4700					
	μ_n (MPa)	α_n	μ_n (MPa)	α_n	μ_n (MPa)	α_n
$N=1$	0.8716	2.340	6.958×10^{-3}	7.954	0.03046	5.381
$N=2$	−0.2815	−6.698	−0.3318	−6.047		
	G_m (MPa)	β_m (/s)	G_m (MPa)	β_m (/s)	G_m (MPa)	β_m (/s)
$M=1$	2.571	8.086	1.189	3.750×10^{-3}	1.732	1.037×10^{-3}
$M=2$	0.9873	0.4183	0.8255	0.5305	0.6344	0.1652
$M=3$			2.661	6.136	1.24	0.5783
$M=4$					0.0881	4.2933
$M=5$					1.740	5.316
	Optimal values of the material parameters for the IM800A					
	μ_n (MPa)	α_n	μ_n (MPa)	α_n	μ_n (MPa)	α_n
$N=1$	2.044	1.562	1.363	1.664	0.05349	4.229
$N=2$			−0.09025	−6.642		
	G_m (MPa)	β_m (/s)	G_m (MPa)	β_m (/s)	G_m (MPa)	β_m (/s)
$M=1$	0.2691	0.9391	0.2480	0.02602	1.496	7.162×10^{-4}
$M=2$			0.3587	2.974	0.2875	0.1404
$M=3$					0.3168	0.9253

Table 3 Percentage deviations in L^2-norm between the experimental and the predicted stress, stretch, and strain-rate curves. Numbers are in italics when the experimental data was not considered for the least-squares fit.

		DFA4700			IM800A		
Stress–stretch curve	Strain rate $\dot{\varepsilon}^{\mathrm{Eng}}$	Case 1	Case 2	Case 3	Case 1	Case 2	Case 3
Compression	−0.001/s	12.2	10.2	16.1	9.52	3.92	7.82
Tension cycle 1 loading	0.01/s	7.01	10.7	24.0	3.17	4.53	12.6
Tension cycle 1 unloading		*27.0*	4.61	20.3	*15.1*	2.56	10.1
Tension cycle 2 loading		*32.1*	*142*	16.0	*7.85*	*9.65*	10.3
Tension cycle 2 unloading		*88.3*	*223*	18.1	*40.9*	*36.3*	8.98
Tension cycle 1 loading	0.1/s	2.52	5.64	12.6	3.00	4.68	8.14
Tension cycle 1 unloading		*19.3*	12.9	18.6	*8.25*	5.56	6.93
Tension cycle 2 loading		*20.2*	*125*	12.5	*3.70*	*5.13*	8.19
Tension cycle 2 unloading		*75.8*	*218*	25.3	*31.5*	*33.4*	14.0
Tension cycle 1 loading	0.5/s	3.39	6.74	12.0	1.25	2.14	3.71
Tension cycle 1 unloading		*18.0*	9.92	15.5	*4.35*	2.54	6.14
Tension cycle 2 loading		*20.2*	*79*	17.7	*5.82*	*3.69*	5.71
Tension cycle 2 unloading		*55.4*	*160*	22.7	*20.4*	*25.7*	12.3
Tension cycle 1 loading	1.0/s	3.65	6.31	10.7	4.00	3.48	7.49
Tension cycle 1 unloading		*14.7*	*8.26*	14.6	*8.38*	*3.27*	7.79
Tension	5.0/s	2.26	*2.35*	4.79	3.33	*2.64*	5.67

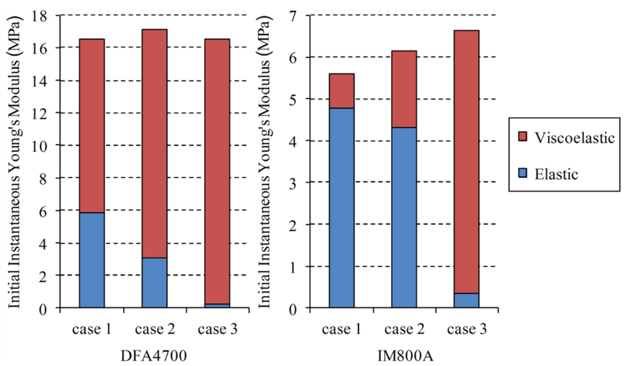

Fig. 3 Contributions to the small-strain instantaneous Young's modulus from the elastic and the viscoelastic parts of the constitutive relation

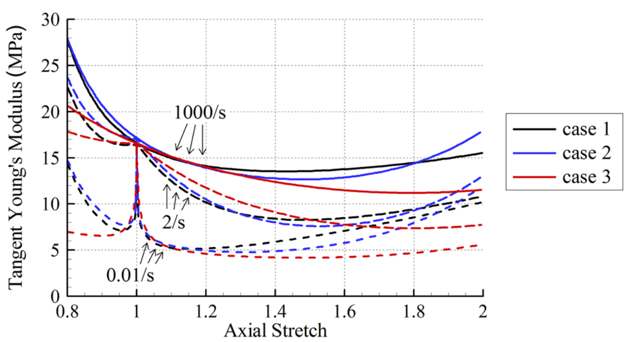

Fig. 4 Predicted tangent modulus as a function of the axial stretch for the DFA4700 material

cycle does not imply that the agreement with the second cycle is also improved.

For small strains, the instantaneous Young's modulus E_0 of the material is given by

$$E_0 = \frac{3}{2}\sum_{n=1}^{N}\mu_n\alpha_n + \sum_{m=1}^{M}3G_m \tag{12}$$

where the first term on the righthand side is due to the contribution from $\boldsymbol{\sigma}^{\mathrm{nlel}}$ derived from W, and the second term corresponds to the

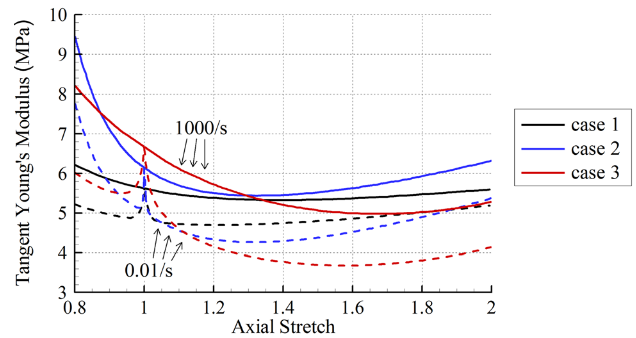

Fig. 5 Predicted tangent modulus as a function of the axial stretch for the IM800A material

contribution from $\boldsymbol{\sigma}^{\mathrm{ve}}$. In Fig. 3, we have exhibited contributions from the elastic and the viscoelastic responses to the initial instantaneous Young's modulus of the DFA4700 and the IM800A materials. It is clear from the results that when test data from more cycles are considered to find values of material parameters the contribution from the elastic part of the constitutive relation to the initial shear modulus decreases. The decrease is especially large for cases 2 and 3 for which test data for complete cycle 1, and complete first two cycles is considered for finding values of material parameters. One should note that the contribution to the stress from $\boldsymbol{\sigma}^{\mathrm{nlel}}$ is not negligible at large strains, since the hardening parameters α_n have large values. The results depicted in Fig. 3 follow from the observation that if more cycles are considered and consequently the final time of the test becomes large a part of the response that was initially considered nonlinear elastic has more time to relax and gets incorporated into the viscoelastic response via additional terms in the Prony series that have small decay constants (i.e., large relaxation times).

In Figs. 4 and 5, we have plotted the tangent Young's modulus for uniaxial tension or compression (computed as $\partial\sigma^{\mathrm{True}}_{\mathrm{I,load}}/\partial\lambda$ with different values of $\dot{\varepsilon}^{\mathrm{Eng}}(=\dot{\lambda})$ and λ) as a function of the axial stretch λ for different strain rates. The highest strain rate considered is 10^3/s, since curves for higher strain rates would be superimposed. It is interesting to note that for low strain rates, the tangent Young's modulus initially decreases with a change in the value of the axial stretch from 1 or equivalently small axial strains. However, this is not the case for axial engineering strain rates higher than 10/s. Also, the tangent modulus at a constant engineering strain rate is a function of the stretch. Even for small strains, the tangent modulus is a different function of the

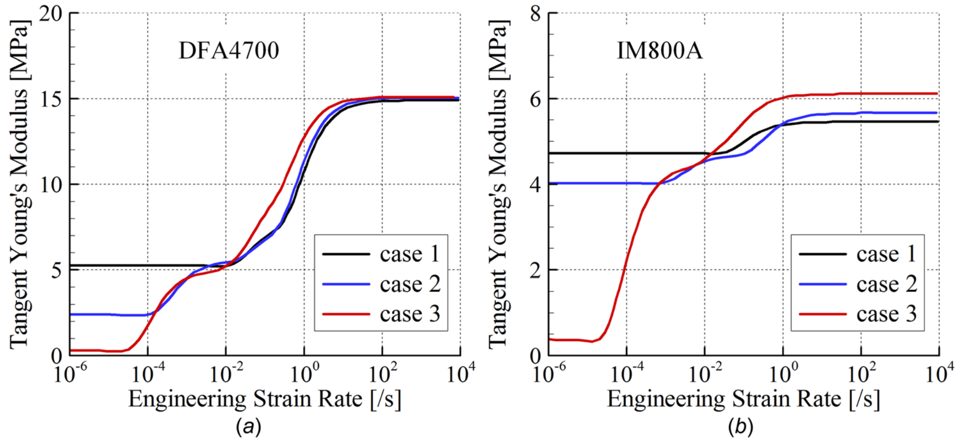

Fig. 6 Predicted tangent modulus at 10% engineering strain ($\lambda = 1.1$) as a function of the engineering strain rate $\dot{\varepsilon}^{\mathrm{Eng}} = \dot{\lambda}$

magnitude of the axial strain for compressive and tensile deformations except for large values of the axial strain rate.

In Fig. 6, we have exhibited the tangent Young's modulus in uniaxial tension $\partial\sigma^{\mathrm{True}}_{1,\mathrm{load}}/\partial\lambda$ for $\lambda = 1.1$ as a function of the strain rate of the deformation $\dot{\varepsilon}^{\mathrm{Eng}} = \dot{\lambda}$ and for the different fitting methods used. The choice $\lambda = 1.1$ is motivated by the large change in the value of the predicted tangent moduli for this value of stretch (see Figs. 4 and 5). These plots clearly show that the strain-rate sensitivity of the proposed constitutive relation increases when data for more loading cycles are considered in finding values of material parameters. One should note that the range of strain rates in the experimental data used for the three cases is not the same (-0.001/s in compression and 0.01 to 5/s in tension). The high strain rate stiffness of the materials is much less affected by the fitting method than its low strain rate response. This is because terms with small decay constants are added to the Prony series when more deformation cycles are included.

The experimental stress–axial stretch curves are given, respectively, in Figs. 7 and 8 for the DFA4700 and the IM800A materials as well as the corresponding model predictions for the three methods of finding values of material parameters.

The statement made earlier that the agreement between the model predictions and the experimental results for the second deformation cycle is not necessarily improved by including data from the unloading part of the first cycle (case 2 compared to case 1) is obvious from results depicted in Fig. 7. Moreover, we see that predictions of model 1 exhibit a very small hysteresis, since the curves corresponding to loading and unloading are almost superimposed. We also note that the blue curves (case 1) are in close agreement with the loading part of the first cycle while they do not capture the unloading part and the second cycle. Similar remarks hold for the IM800A adhesive (Fig. 8). We see that for both adhesives the agreement between the green curves (case 3) and the experimental data for the second deformation cycle is not very good, and in particular the area within the hysteresis loop (which is related to the energy dissipation) is underestimated. This is a limitation of the proposed constitutive relation, since no values of material parameters could be found that improved the correlation between the test data and the model predictions for cyclic loading.

Loss and Storage Moduli. To find expressions for the storage and the loss moduli as a function of the frequency of the deformation, we first derive an expression for the axial stress as a function of the axial strain for small strains which are typical of dynamic mechanical analysis (DMA) experiments. We linearize Eq. (A28) of the Appendix for small strains for which there is no distinction

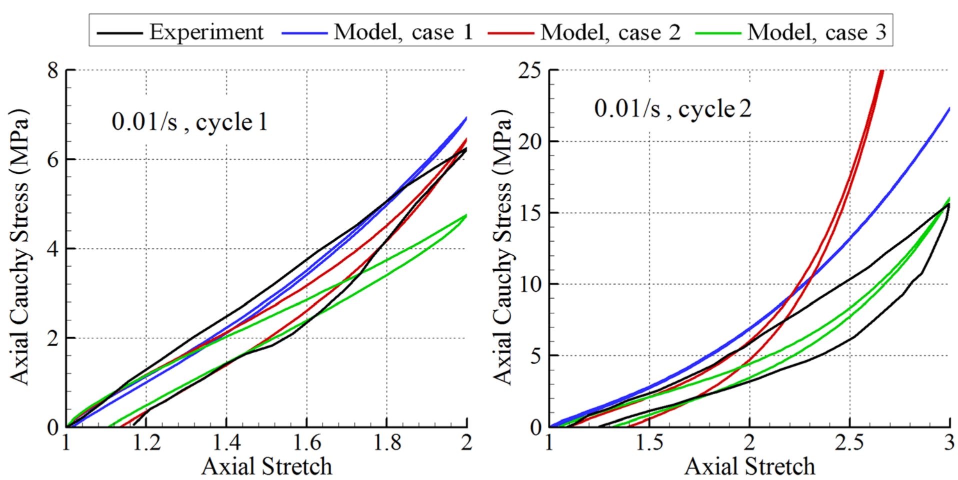

Fig. 7 Experimental and predicted true axial stress as a function of the axial stretch for cyclic tensile deformations of DFA4700 at 0.01/s

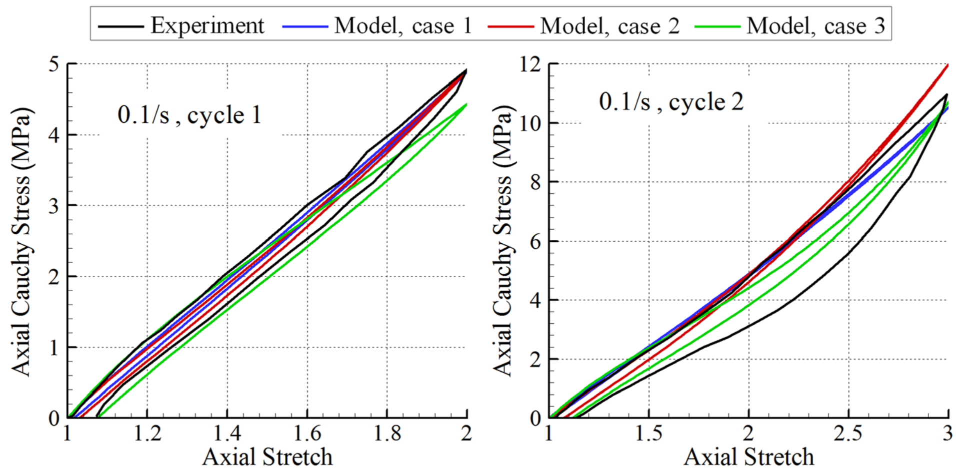

Fig. 8 Experimental and predicted true axial stress as a function of the axial stretch for cyclic tensile deformations of IM800A at 0.1/s

between the true and the engineering strains, strain rates, and stresses and obtain the following axial stress–axial strain relation:

$$\sigma(t) = \left(\sum_{n=1}^{N} \frac{3}{2}\mu_n\alpha_n\right)\varepsilon(t) + \sum_{m=1}^{M}\sigma_m(t) \tag{13a}$$

$$\sigma_m(t) = 3G_m \int_{\tau=0}^{t} e^{-\beta_m(t-\tau)}\dot{\varepsilon}(\tau)d\tau \tag{13b}$$

Equation (13b) is equivalent to the following differential equation:

$$\dot{\sigma}_m(t) = 3G_m\dot{\varepsilon}(t) - \beta_m\sigma_m(t) \tag{14}$$

In terms of complex variables indicated below by a superimposed hat, we define the complex axial strain $\bar{\varepsilon}$ and the complex axial stresses $\bar{\sigma}$ and $\bar{\sigma}_m$ as

$$\begin{aligned} \varepsilon(t) &= \mathrm{Re}(\bar{\varepsilon}(t)), \quad \bar{\varepsilon}(t) = \hat{\varepsilon}e^{i\omega t} \\ \sigma(t) &= \mathrm{Re}(\bar{\sigma}(t)), \quad \bar{\sigma}(t) = \hat{\sigma}e^{i\omega t} \\ \sigma_m(t) &= \mathrm{Re}(\bar{\sigma}_m(t)), \quad \bar{\sigma}_m(t) = \hat{\sigma}_m e^{i\omega t} \end{aligned} \tag{15}$$

By substituting from Eq. (15) into Eq. (14), we obtain the following relation between $\hat{\sigma}_m$ and $\hat{\varepsilon}$ featuring the loss and the storage moduli, $E'_m(i\omega)$ and $E''_m(i\omega)$, corresponding to the mth term of the Prony series:

$$\begin{aligned} \hat{\sigma}_m &= E'_m(i\omega)\hat{\varepsilon} + iE''_m(i\omega)\hat{\varepsilon}, \\ E'_m(i\omega) &= \frac{3G_m}{1+(\beta_m/\omega)^2}, \\ E''_m(i\omega) &= \frac{3G_m}{\dfrac{\beta_m}{\omega}+\dfrac{\omega}{\beta_m}} \end{aligned} \tag{16}$$

Equations (13)–(16) give

$$\hat{\sigma} = E'(i\omega)\hat{\varepsilon} + iE''(i\omega)\hat{\varepsilon} \quad \text{with}$$
$$\begin{cases} E'(i\omega) = \displaystyle\sum_{n=1}^{N}\frac{3}{2}\mu_n\alpha_n + \sum_{m=1}^{M}\frac{3G_m}{1+(\beta_m/\omega)^2} \\ E''(i\omega) = \displaystyle\sum_{m=1}^{N}\frac{3G_m}{\dfrac{\beta_m}{\omega}+\dfrac{\omega}{\beta_m}} \end{cases} \tag{17}$$

In Fig. 9, we have depicted the storage modulus and $\tan(\delta) = E''/E'$ as a function of the angular frequency ω of the deformation for the two materials and for different methods of finding values of the material parameters described above. Note that the shear storage and loss moduli $G'(i\omega)$ and $G''(i\omega)$ are related to Young's storage and loss moduli $E'(i\omega)$ and $E''(i\omega)$ by $G'(i\omega) = E'(i\omega)/(2(1+\nu)) = E'(i\omega)/3$ and $G''(i\omega) = E''(i\omega)/3$, since the materials are incompressible and the deformations are small.

For the DFA4700, the model predicted values of the storage and the loss moduli for $f > 10$ Hz and cases 1, 2, and 3 do not show any significant differences. The storage modulus predicted at high frequencies for case 2 is about 17.2 MPa, while it is 16.6 MPa for the two other cases considered (3.6% difference). For the IM800A adhesive and $f > 10$ Hz, the predicted values of the storage moduli vary between 5.60 MPa (case 1) and 6.64 MPa (case 3), which gives a difference of approximately 19%. Besides these observations, the largest difference in the predictions is the following: the consideration of the first unloading and of the second complete deformation cycle in the data used to find values of material parameters causes a large difference in the very low strain-rate ($<10^{-4}$ Hz) response of the material. This is true for both materials, and for DFA4700 (IM800A), the predicted storage modulus at very low strain-rates is 5.88 MPa (4.79 MPa) in case 1, 3.11 MPa (4.31 MPa) in case 2, and 0.23 MPa (0.343 MPa) in case 3. This gives a factor of 25 and 14 between the quasi-static storage moduli of cases 1 and 3 for the DFA4700 and the IM800A, respectively. Moreover, we notice that for both adhesives values of material parameters found in case 3 introduce a very large peak in the value of the tangent delta at low strain rates, since the tangent delta is greater than one for some frequencies, which means that at those frequencies the loss modulus is greater than the storage modulus. Since the storage modulus at very low strain-rates is the small strain Young's modulus of the nonlinear elastic response of the material (see Eq. (17) when $\omega \to 0$) this is consistent with the remarks made for results shown in Fig. 3.

Stenzler [23] performed DMA of DFA4700 and IM800A samples at 1 Hz for temperatures between -150 and $+100\,^\circ$C. From the experimental results, one can read the $\tan(\delta)$ at room temperature (assumed to be $20 \pm 5\,^\circ$C) for imposed cyclic deformation at 1 Hz. These values are compared to the corresponding model predictions in Table 4.

With the material parameters found in cases 1 and 2, the predicted value of $\tan(\delta)$ for the DFA4700 is comparable to the experimental value. However, in case 3, the predicted value is about 40% smaller than that obtained from the DMA data. For the IM800A adhesive, the predicted values are far smaller than the

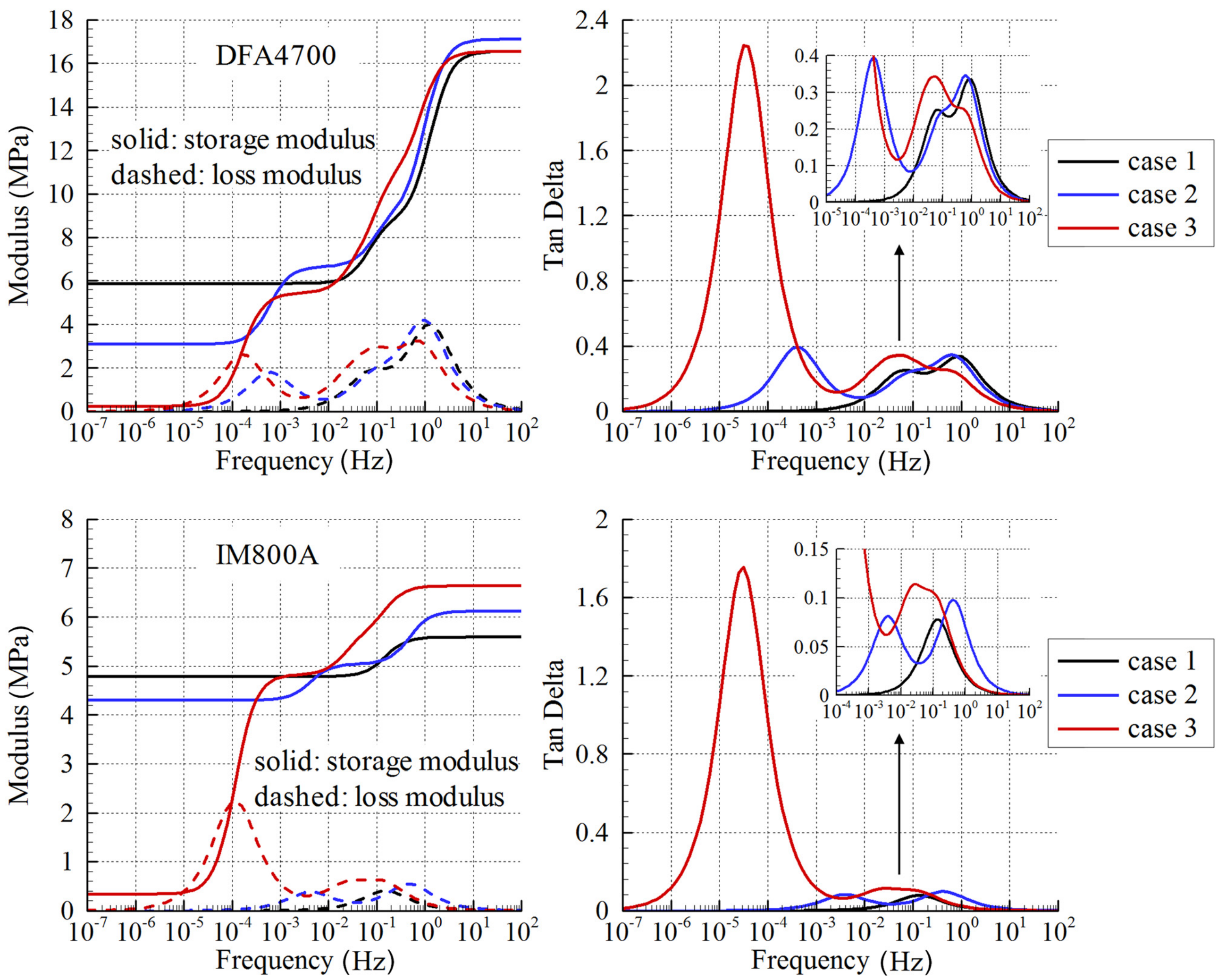

Fig. 9 Storage modulus, loss modulus, and tangent delta as a function of the frequency $f = \omega/(2\pi)$ for uniaxial deformations. Note that the frequency is plotted by using the logarithmic scale.

Table 4 Comparison of experimental and predicted values of tan(δ) at room temperature ($20 \pm 5\,^\circ$C) and 1 Hz loading rate

		Predicted tan(δ)		
Material	Experimental tan(δ)	Case 1	Case 2	Case 3
DFA4700	0.37 ± 0.04	0.34	0.32	0.22
IM800A	0.11 ± 0.02	0.021	0.071	0.023

experimental ones in all three cases. We note that the experimental tan(δ) of the IM800A is quite small and corresponds to a 6.3 ± 1.1 deg phase difference between the prescribed stress and the measured strain.

When test data for case 3 is used to find values of material parameters, the constitutive relation shows the most rate sensitivity and the predicted tan(δ) for 1 Hz at room temperature is smaller than that found for cases 1 and 2. This is because most of the strain-rate dependency for case 3 occurs at very low frequencies in Fig. 9 the peak in the value of tan(δ) occurs at 10^{-5}–10^{-4} Hz frequencies. These results suggest that by improving the agreement between the model predictions and the experimental data for the second cycle of deformations the model predictions for the first deformation cycles are worsened. A large part of the viscoelastic response of the material is attributed to very small relaxation times which results in smaller value of tan(δ) at room temperature and 1 Hz frequency. These remarks are also valid for the IM800A material even though the tan(δ) for it has small values.

Shear Response. We note that for simple shear deformations, the orthogonal matrix $\mathbf{R}$ in the polar decomposition of the deformation gradient F is not identity as it is for uniaxial deformations. Thus, the analysis of the viscoelastic part of the stress–strain curve becomes more interesting. Simple shear deformations in the xy-plane are described by

$$x = X + \gamma Y, \quad y = Y, \quad z = Z \tag{18}$$

where lower (upper) case letters correspond to the position of a material point in the current (reference) configuration, and the shear strain γ is given by $\gamma = \dot{\gamma} t$ with $\dot{\gamma}$ being the constant engineering shear strain rate. The condition $\sigma_{zz} = 0$ is used to determine the hydrostatic pressure. Since $\sigma_{zx} = \sigma_{zy} = 0$, the deformation is plane-stress. The differential equation giving the shear stress σ_{xy} as a function of γ and $\dot{\gamma}$ is integrated numerically using the "NDSolve" function of MATHEMATICA (see the Appendix for more details). The tangent shear modulus calculated as $\partial\sigma_{xy}/\partial\gamma$ is plotted as a function of the shear strain γ for different values of $\dot{\gamma}$ in Fig. 10 for the DFA4700 and in Fig. 11 for the IM800A.

For cases 1 and 2 of the DFA4700 and case 2 of the IM800A—for which there are terms with negative exponents in the strain

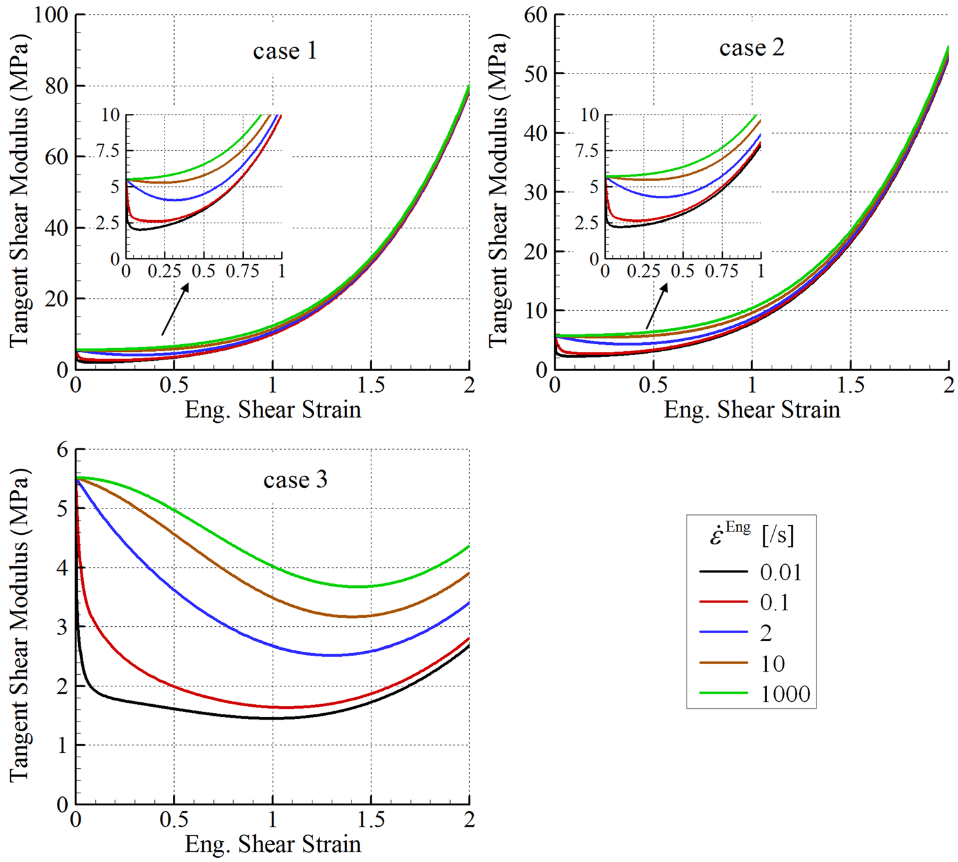

Fig. 10 Predicted tangent shear modulus for simple shear deformations of the DFA4700 material

energy density function W—one can observe that the tangent shear modulus becomes very large at large strains while it remains quite small for the other cases. It is clear that the strain-rate dependency of the DFA4700 material is stronger than that of the IM800A, which is consistent with the results in uniaxial deformation.

The tangent shear modulus is strain rate dependent even for cases 1 and 2 (see insets in the figure) but the scale of the y-axis is so large that it is not obvious in the plots of all of the data. We note that for cases 1 and 2 the tangent shear modulus at high strains has most of the contribution from the nonlinear elastic part of the stress–strain curve which is strain-rate independent. However, for case 3, the contribution to the tangent shear modulus from nonlinear elastic deformations is small which explains the much lower value of the tangent modulus at high strains. Therefore, it appears that having data for shear deformations of adhesives at large shear strains (even for only one strain rate) is essential for capturing the shear response of the adhesive, since the latter is strongly affected by the stored energy function W. However, we note that the deformation field given by Eq. (18) cannot be easily used in experiments, since it leads to nonzero tractions on the material faces orthogonal to the Y-axis in the undeformed configuration, while in a shear lap test (for instance) those boundaries would be free (and the deformation nonuniform). Another possibility is to study the Couette flow between two cylinders.

Discussion of the Constitutive Relations. The proposed constitutive relation does not account for irreversible processes that can take place during large deformations of TPUs such as rearrangement of molecular networks (see Ref. [16]), since when the material is unloaded and $t \rightarrow \infty$ the material completely "forgets" its deformation history as contributions from the Prony series vanish and the material retrieves its original shape. The temperature dependence of material parameters and the relaxation times has not been considered. The latter could be incorporated via the William–Landel–Ferry equation, e.g., see Ref. [24], and assuming that the stored energy function also depends upon the temperature change. These factors may explain why the model cannot well capture the second deformation cycle of the DFA4700 and IM800A. Furthermore, one should compare predictions from the constitutive relation with test data for other types (especially, three-dimensional) of deformation that have not been used to find values of material parameters. However, this has not been done because of the lack of availability of the test data in the open literature.

Ideally, one should consider test data under a variety of loading conditions to find values of material parameters. However, it is not possible since testing materials under controlled conditions and accurately measuring stresses and strains is rather difficult.

The considerable deviation remaining between the predictions and the experimental data of the second deformation cycles in Figs. 7 and 8 are a limitation of the model. Several different initial points (i.e., sets of values) have been used for the least square fitting of the material parameters but all of them eventually yielded values reported in Table 2 of the manuscript (or sets of values giving a worse agreement with experimental data).

For strain-rates varying from 10^{-3} to 10^{3}/s, one probably needs a nonlinear dependence of the Cauchy stress upon the strain-rate tensor. One could potentially include dependence of the Cauchy stress upon $\mathbf{D}^2$, $\mathbf{D}^3$, second invariant of $\mathbf{D}$, and third invariant of $\mathbf{D}$ with the resulting increase in the number of material parameters. Whether or not it will improve correlation between test results and model predictions remains to be explored.

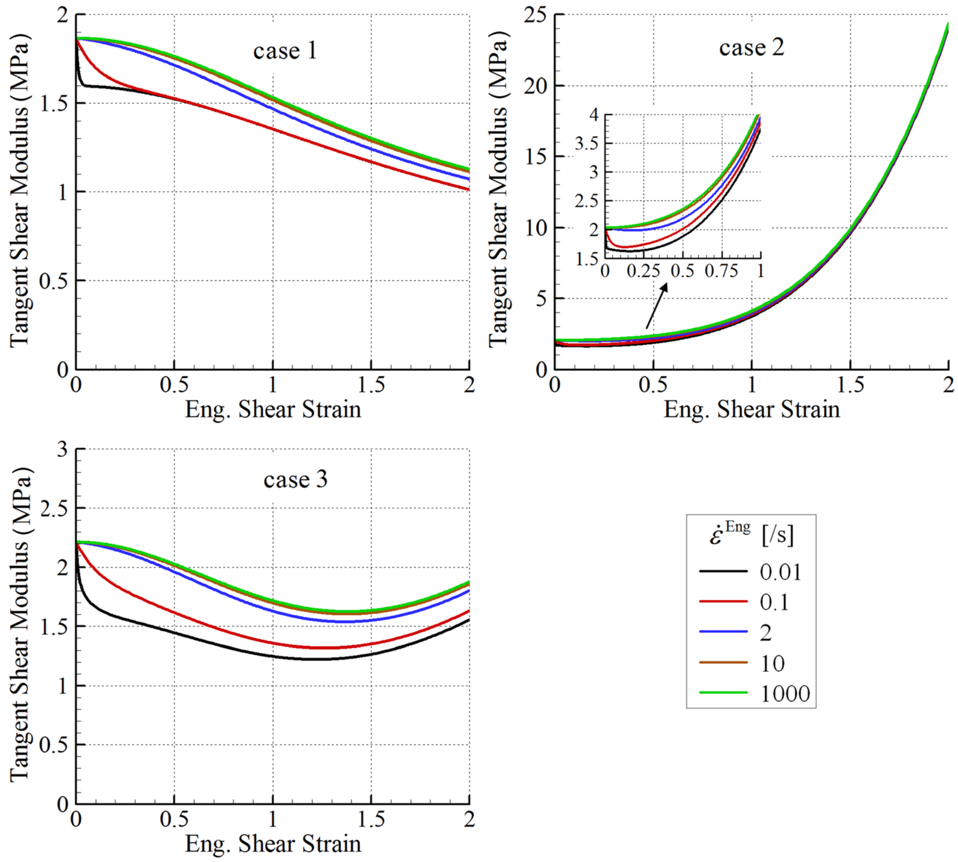

Fig. 11 Predicted tangent shear modulus for simple shear deformations of the IM800A material

We believe that the constitutive relation is applicable for general three-dimensional deformations of rubberlike materials as similar material models have been used for analyzing finite deformations, e.g., see Refs. [15,24].

We note that Yu and Batra [25–27] have studied initial-boundary-value problems with two materially objective constitutive relations that express a stress tensor as a linear function of the time history of the appropriate strain-rate tensor for finite deformations. Whereas the two constitutive relations predict identical results for infinitesimal deformations, they give different results for finite deformations.

The inverse problem of finding values of material parameters for a thermo-elasto-viscoplastic material from the test data by solving initial-boundary-value problems was also studied in Ref. [28].

Application: Simulations of Low-Velocity Impact of Laminate

The constitutive equations presented above have been implemented in the explicit commercial FE software LS-DYNA as a user-defined subroutine. The quasi-static response of the material is computed from the deformation gradient to avoid writing the corresponding constitutive equation in a rate form. For a perfectly incompressible material, the pressure term is a Lagrange multiplier and cannot be determined from deformations of the material (e.g., see Ref. [22]). However, for numerical work, the kinematic constraint of incompressibility is often relaxed and the pressure is simulated by penalizing volumetric strains (e.g., see Ref. [29]). Alternatively, one can use a mixed formulation in which the pressure is an unknown variable and is determined as a part of the solution of the problem, e.g., see Ref. [24]. A mechanical analog of the former approach is depicted in Fig. 12. Thus,

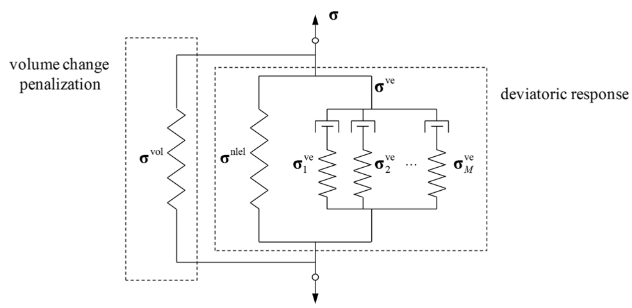

Fig. 12 One-dimensional rheological analog interpretation of the constitutive relation for an incompressible material

$$\boldsymbol{\sigma} = \boldsymbol{\sigma}^{\mathrm{nlel}} + \boldsymbol{\sigma}^{\mathrm{ve}} + \boldsymbol{\sigma}^{\mathrm{vol}} \tag{19}$$

The Cauchy stress $\boldsymbol{\sigma}^{\mathrm{nlel}}$ is found from the following modified strain energy density function:

$$W = \sum_{n=1}^{N} \frac{\mu_n}{\alpha_n}\left(\widetilde{\lambda}_1^{\alpha_n} + \widetilde{\lambda}_2^{\alpha_n} + \widetilde{\lambda}_3^{\alpha_n} - 3\right) \quad \text{where}$$
$$\widetilde{\lambda}_i = \frac{\lambda_i}{(\lambda_1\lambda_2\lambda_3)^{1/3}}, \quad i = 1,2,3 \tag{20}$$

The Cauchy stress $\boldsymbol{\sigma}^{\mathrm{vol}}$ is derived from the strain energy density potential W^{vol} defined in Eq. (21), where J is the Jacobian of the deformation gradient.

$$W^{\mathrm{vol}} = K(J - 1 - \ln(J)) \tag{21}$$

The value of the bulk modulus K must be much greater than that of the shear modulus of the material. In the present work, unless otherwise specified, the value of K has been determined by assuming that the initial Poisson's ratio (at zero strain) of the nearly incompressible material equals 0.4995.

Viscous deformations of the material are assumed to depend only on the deviatoric part $\mathbf{D}^{\text{dev}}$ of the strain rate tensor.

$$\boldsymbol{\sigma}^{\text{ve}} = \sum_{m=1}^{M} \boldsymbol{\sigma}_m^{\text{ve}}, \quad \begin{cases} \overset{\bullet}{\boldsymbol{\sigma}}{}_m^{\text{ve}} = 2G_m \mathbf{D}^{\text{dev}} - \beta_m \boldsymbol{\sigma}_m^{\text{ve}} \\ \boldsymbol{\sigma}_m^{\text{ve}}\big|_{t=0} = 0 \end{cases} \tag{22}$$

The energy dissipated per unit current volume due to viscous effects $E^{\text{visc,ve}}$ is calculated at each time step in the user defined material subroutine, and the total energy dissipated due to viscous deformations is obtained by integrating over the deformed volume (i.e., by summing elemental contributions).

The impact problem studied here, shown schematically in Fig. 13, is the same as that analyzed by Antoine and Batra [19] where a complete description of the problem, the mathematical model, and details of the computational work are described. The difference between that work and the one reported here is in the constitutive relations of the DFA4700 and the IM800A and values of material parameters. Here, results have been computed for the three sets of test data used to find values of material parameters for the two adhesives.

For the sake of completeness, we give a brief description of the material model for the PC and the PMMA. The same set of constitutive equations is used for the two materials, only values of the material parameters differ. We assume that the Cauchy stress $\boldsymbol{\sigma}$ is the sum of a nonlinear elastic contribution $\boldsymbol{\sigma}_{\text{B}}$ (restoring force from phase B) and of two viscoelastoplastic contributions $\boldsymbol{\sigma}_\alpha$ and $\boldsymbol{\sigma}_\beta$ (from phases α and β), i.e., $\boldsymbol{\sigma} = \boldsymbol{\sigma}_{\text{B}} + \boldsymbol{\sigma}_\alpha + \boldsymbol{\sigma}_\beta$. The contribution of phase B is

$$\boldsymbol{\sigma}_{\text{B}} = \frac{C_R}{3} \frac{\sqrt{N_l}}{\lambda^{\text{p}}} L^{-1}\left(\frac{\lambda^{\text{p}}}{N_l}\right) \overline{\mathbf{B}'}_{\text{B}} \tag{23}$$

Here, $\overline{\mathbf{B}'}_{\text{B}}$ is the deviatoric part of $\overline{\mathbf{B}}_{\mathbf{B}} = (J)^{-2/3}\mathbf{F}\mathbf{F}^{\mathbf{T}}$, $\lambda^{\text{p}} = \sqrt{\text{tr}\left(\overline{\mathbf{B}}_{\mathbf{B}}\right)/3}$, L^{-1} is the inverse of the Langevin function $L(\beta) \equiv \coth\beta - 1/\beta$, N_l is the limiting stretch, $C_{\text{R}} \equiv n_{\text{R}} k\theta$, θ is the temperature in Kelvin, k is Boltzmann's constant, and n_{R} a material parameter.

The constitutive equations of the two other phases α and β rely on the decomposition of the deformation gradient into elastic and plastic parts, e.g., see Refs. [30] and [31].

$$\mathbf{F} = \mathbf{F}_\alpha^{\text{e}} \mathbf{F}_\alpha^{\text{p}} = \mathbf{F}_\beta^{\text{e}} \mathbf{F}_\beta^{\text{p}} \tag{24}$$

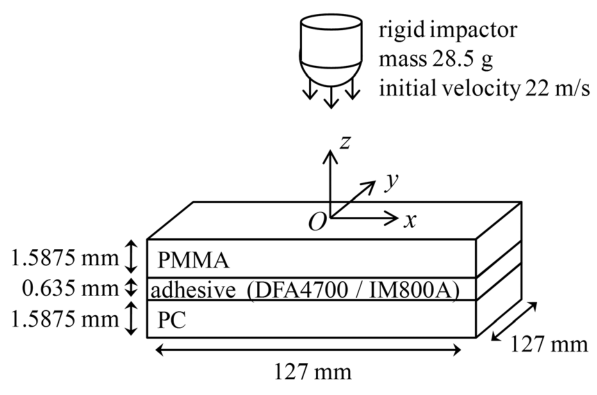

Fig. 13 Schematic sketch of the impact problem studied

The rate of the plastic deformation gradient is given by

$$\dot{\mathbf{F}}_\alpha^{\text{p}} = \mathbf{F}_\alpha^{\text{e}^{-1}} \widetilde{\mathbf{D}}_\alpha^{\text{p}} \mathbf{F}, \quad \dot{\mathbf{F}}_\beta^{\text{p}} = \mathbf{F}_\beta^{\text{e}^{-1}} \widetilde{\mathbf{D}}_\beta^{\text{p}} \mathbf{F}, \tag{25}$$

where $\widetilde{\mathbf{D}}_i^{\text{p}}$ is the plastic stain-rate tensor in phase $i = \alpha, \beta$ (It has been assumed that the plastic spin tensors are identically zero.)

The Hencky elastic strain tensor and the Cauchy stress tensor in phase $i = \alpha, \beta$ are given by

$$\boldsymbol{\varepsilon}_i^{\text{e}} = \ln\left(\sqrt{\mathbf{F}_i^{\text{e}} \mathbf{F}_i^{\text{e}^{\text{T}}}}\right), \quad \boldsymbol{\sigma}_i = \frac{1}{\det\left(\mathbf{F}_i^{\text{e}}\right)}\left[2\mu_i \boldsymbol{\varepsilon}_i^{\text{e}} + \lambda_i \text{tr}(\boldsymbol{\varepsilon}_i^{\text{e}})\mathbf{1}\right] \tag{26}$$

The plastic rate-of-strain tensors in phases α and β are collinear with the deviatoric Cauchy stress tensor of their respective phases and have magnitude $\dot{\gamma}_i^{\text{p}}$ given by

$$\dot{\gamma}_i^{\text{p}} = \dot{\gamma}_{0i}^{\text{p}} \exp\left[-\frac{\Delta G_i}{k\theta}\left(1 - \frac{\tau_i}{t_i \hat{s}_i + \alpha_i^{\text{p}} p}\right)\right] \tag{27}$$

Here, $\dot{\gamma}_{0i}^{\text{p}}$, ΔG_i, α_i^{p} are material parameters, $\tau_i = \sqrt{0.5\text{tr}\left(\boldsymbol{\sigma}_i'\boldsymbol{\sigma}_i'\right)}$, $\hat{s}_i = 0.077\mu/(1-\nu_i)$ where ν_i is Poisson's ratio of phase $i = \alpha, \beta$, $p = -\text{tr}(\boldsymbol{\sigma})/3$, t_i is an internal variable whose initial value is 1.0 and whose evolution is described by

$$\dot{t}_i = \frac{h_i}{\hat{s}_i^0}\left(1 - \frac{t_i}{t_i^{\text{ss}}}\right)\dot{\gamma}_i^{\text{p}} \tag{28}$$

The energy dissipated by plastic deformations is converted into heat and deformations are assumed to be adiabatic (which is a reasonable assumption for impact problems) resulting in Eq. (29) for the rate of change of temperature, $\dot{\theta}$.

$$\rho_0 c\dot{\theta} = \dot{Q} = J \cdot \left(\boldsymbol{\sigma}_\alpha : \widetilde{\mathbf{D}}_\alpha^{\text{p}} + \boldsymbol{\sigma}_\beta : \widetilde{\mathbf{D}}_\beta^{\text{p}}\right) \tag{29}$$

Table 5 Values of material parameters for the PC

	Phase α	Phase β	Phase B	Common
ν_i	0.38	0.38		
$\dot{\gamma}_{0i}^{\text{p}}$ (/s)	2.94×10^{16}	3.39×10^{5}		
ΔG_i (J)	3.744×10^{-19}	3.769×10^{-20}		
α_i^{p}	0.168	0.245		
h_i (MPa)	125	400		
t_i^{ss}	0.33	2.00		
C_{R} at 300 K (MPa)			35.0	
N_l			12.25	
c (J/(g·K))				1.20
ρ (g/cm^3)				1.20
E (GPa) at 300 K, 5000/s	1.678	0.344		

Table 6 Values of material parameters for the PMMA

	Phase α	Phase β	Phase B	Common
ν_i	0.35	0.35		
$\dot{\gamma}_{0i}^{\text{p}}$ (/s)	6.95×10^{219}	1.77×10^{3}		
ΔG_i (J)	5.528×10^{-18}	6.036×10^{-20}		
α_i^{p}	0.260	0.260		
h_i (MPa)	200	500		
t_i^{ss}	0.73	0.45		
C_{R} at 300 K (MPa)			14.0	
N_l			2.10	
c (J/(g·K))				1.46
ρ (g/cm^3)				1.14
E (GPa) at 300 K, 5000/s	2.604	1.748		

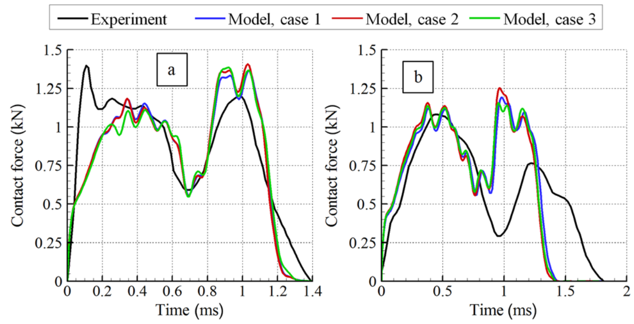

Fig. 14 Time histories of the experimental [23] and the computed contact force for the impact of the (*a*) PMMA/DFA4700/PC and (*b*) PMMA/IM800A/PC plates

In Eq. (29), c is the specific heat of the material, and ρ_0 is the initial mass density.

Values of material parameters and approximate values of Young's moduli of phases α and β are given in Table 5 for the PC and in Table 6 for the PMMA.

In Fig. 14, time histories of the contact force for the normal incidence impact of the clamped PMMA/DFA4700/PC and the PMMA/IM800A/PC plates at 22 m/s by a 28.5 g hemispherical-nosed rigid impactor are depicted. The closeness of the numerical results for the three sets of values of material parameters is consistent with those depicted in Fig. 6 which shows that the response of the interlayer material at high strain rates (which are typical of the impact problem) is essentially independent of the method used to find values of material parameters. We now comment on the experimental value of the peak contact force at 0.1 ms. For each laminate and the impact velocity, Stenzler [23] conducted three tests but gave only one curve ("Representative force and displacement traces are given for each interlayer and velocity" [23]). For the PMMA/DFA4700/PC assembly and 22 m/s impact velocity he did not mention if the peak in the contact force at 0.1 ms was present in all three experiments. Stenzler [23] provided in the Appendix of his thesis a summary of the characteristics of the reaction force history. There in the column "first force peak" and row "PMMA/DFA4700/PC, 22.7 m/s" is written 1.14 kN, which does not correspond to the peak value of 1.4 kN at 0.1 ms shown in the figure, but to the value of the contact force at about 0.3 ms. It thus appears that this peak in the contact force did not occur in all of the three tests.

The postimpact fracture patterns in the PMMA layer are shown in Fig. 15 (Fig. 16) for plates with the DFA4700 (the IM800A) interlayer.

The fracture patterns are qualitatively and quantitatively similar for cases 1, 2, and 3 for both adhesives. We observe that the circular-shaped cracks near the center of impact in the PMMA layers have essentially the same radii, except for the IM800A adhesive and case 1 in which no such pattern formed. Moreover, the in-plane extension of cracks is the same as also evidenced by the time histories of the computed maximum in-plane extension of a

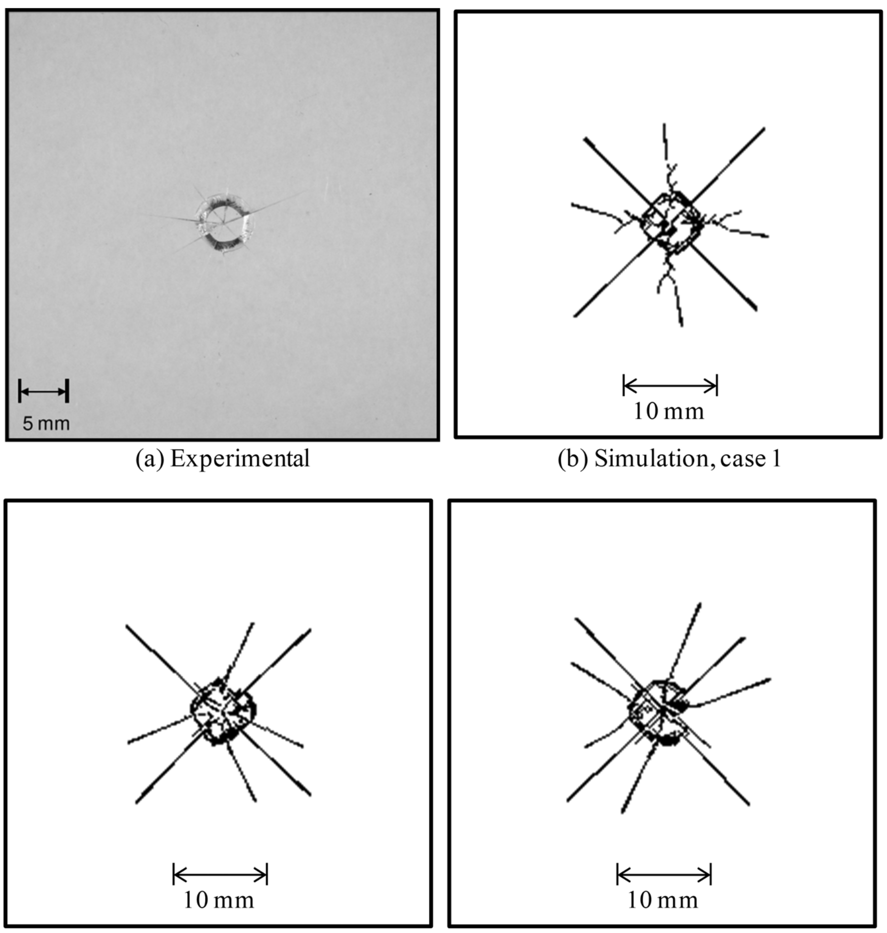

(a) Experimental (b) Simulation, case 1 (c) Simulation, case 2 (d) Simulation, case 3

Fig. 15 (*a*) Experimental (from Ref. [23]) and simulated ((*b*)–(*d*)) postimpact crack patterns in the PMMA layer of the PMMA/DFA4700/PC assembly impacted at 22 m/s. The three sets of material parameters for the DFA4700 interlayer are used in the simulations.

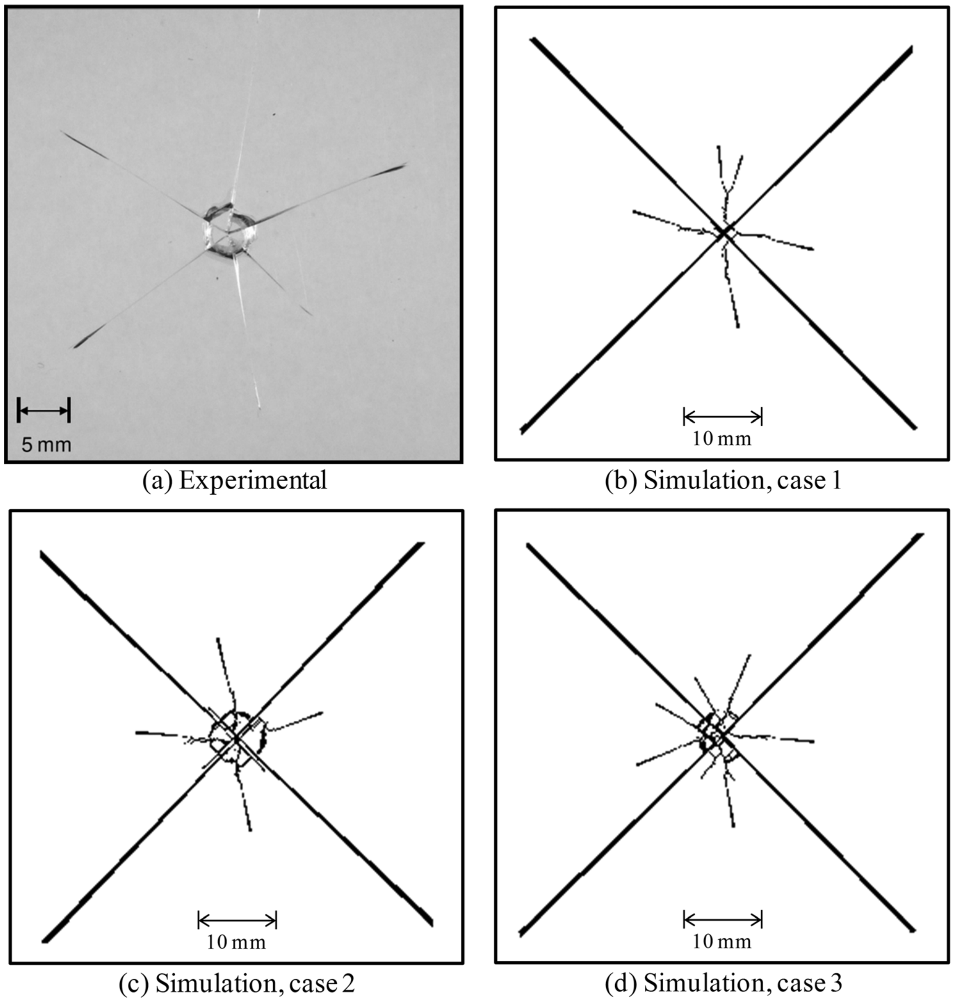

Fig. 16 (*a*) Experimental (from Ref. [23]) and simulated ((*b*)–(*d*)) postimpact crack patterns in the PMMA layer of the PMMA/IM800A/PC assembly impacted at 22 m/s. The three sets of material parameters for the IM800A interlayer are used in the simulations.

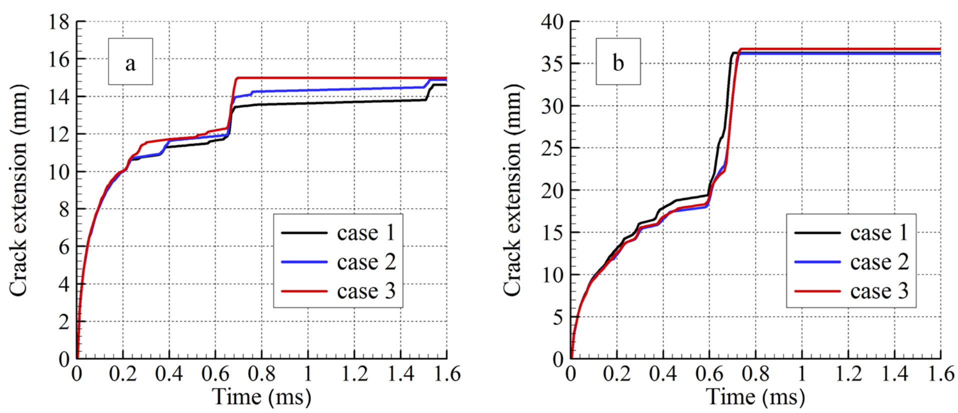

Fig. 17 Time histories of the in-plane extension of cracks formed in the PMMA layer for the normal impact of the (*a*) PMMA/DFA4700/PC and (*b*) PMMA/IM800A/PC plates

crack in the PMMA plate provided in Fig. 17. We note that no such experimental data are available.

The principal sources of energy dissipation for the impact problem are the "eroded energy" due to the material failure and the subsequent crack formation in the PMMA layer, the energy due to plastic deformations of the PMMA and the PC layers, and the energy of viscous deformations of the adhesive interlayer. Their values in mJ are listed in Table 7. We note that the kinetic and the strain energies of the PMMA, the PC, and the adhesive layers are not listed in the table. The energy dissipated due to viscous deformations of the adhesive is a miniscule part of the kinetic energy of the impactor. For the DFA4700 (IM800A), the choice of the set of material parameters for the adhesive used in the simulations induces a variation in the energy dissipated due to cracking of the

Table 7 Impact energy and sources of energy dissipation for the impact of the laminated plates. Energies are given in mJ.

	PMMA/DFA4700/PC plate			PMMA/IM800A/PC plate		
	Case 1	Case 2	Case 3	Case 1	Case 2	Case 3
Initial kinetic energy of impactor	6900	6900	6900	6900	6900	6900
Final kinetic energy of impactor	4620	4640	4620	4830	4730	4760
Energy due to cracking of PMMA	210	189	195	238	280	261
Energy of plastic deformations of the PMMA	18.1	18.9	20.3	29.5	21.3	26.4
Energy due to viscous deformations of the adhesive	6.33	4.92	3.43	0.288	0.965	0.318
Energy of plastic deformations of the PC	794	846	867	817	785	810
Total energy dissipated	1028	1059	1086	1085	1087	1098

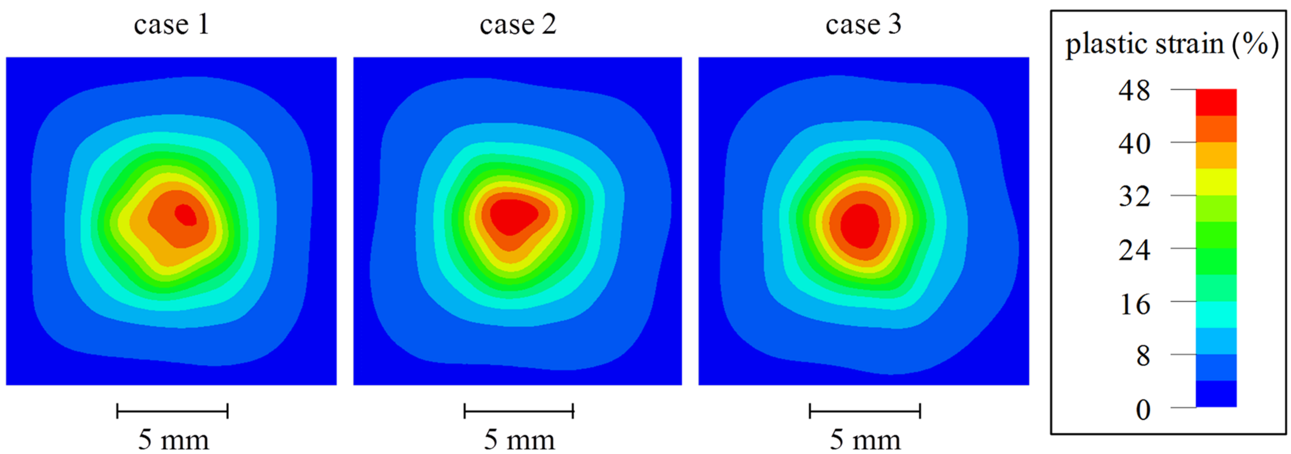

Fig. 18 Fringe plots of the effective plastic strain near the center of the back surface of the PC layer of the PMMA/DFA4700/PC laminate

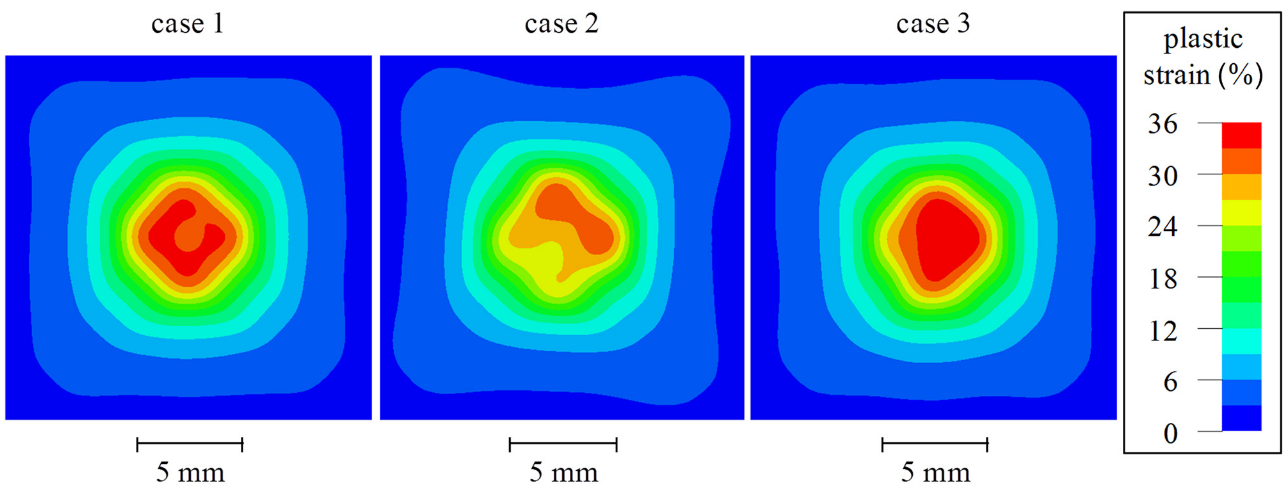

Fig. 19 Fringe plots of the effective plastic strain near the center of the back surface of the PC layer of the PMMA/IM800A/PC laminate

PMMA layer of about 11% (19%). The energy dissipated due to plastic deformations of the PC layer varies by about 10% (4%) for the laminate using DFA4700 (IM800A). As expected, values of material parameters for the adhesive noticeably influence the energy dissipated due to viscous deformations of the adhesive interlayer. However, energies dissipated due to deformations of the adhesive are negligible as compared to that due to plastic deformations of the PC layer. The energy dissipated due to cracking and plastic deformations of the PMMA layer is approximately one-fourth of that due to plastic deformations of the PC layer.

For the three sets of values of material parameters for the two adhesives, contours of the plastic strain on the back face of the PC layer are not much affected either qualitatively or quantitatively, as shown in Figs. 18 and 19.

The results given in Table 7 imply that the energy due to viscous dissipation does not increase between cases 1 and 3, which seems to contradict results included in Fig. 3 that indicate that the viscoelastic contribution to the instantaneous elastic response of the materials increases. In order to investigate this further, we assume that relaxation effects are negligible (i.e., $\|2G_m\mathbf{D}^{\text{dev}}\| \gg \|\beta_m\boldsymbol{\sigma}_m^{\text{ve}}\|$ for all m, deformations are isochoric (i.e., $J=1$), and rotation effects are negligible (i.e., the deformation gradient $\mathbf{F}$ is nearly symmetric). These assumptions imply that $\boldsymbol{\sigma}_m^{\text{ve}} \approx 2G_m\boldsymbol{\varepsilon}^{\text{dev}}$, where $\boldsymbol{\varepsilon}^{\text{dev}}$ is the deviatoric part of the Hencky

Table 8 Normalized energy dissipations found by using Eqs. (31) and (32). Deviations between $\hat{E}_m^{\text{visc,ve}}$'s and $\hat{\varepsilon}$ are given in parentheses (using the $\hat{E}_m^{\text{visc,ve}}$'s as reference values).

PMMA/DFA4700/PC	Case 1	$\hat{\varepsilon}$	0.0845
		$\hat{E}_1^{\text{visc,ve}}$	0.0829 (+1.9%)
		$\hat{E}_2^{\text{visc,ve}}$	0.0832 (+1.6%)
	Case 2	$\hat{\varepsilon}$	0.0841
		$\hat{E}_1^{\text{visc,ve}}$	0.0827 (+1.7%)
		$\hat{E}_2^{\text{visc,ve}}$	0.0827 (+1.7%)
		$\hat{E}_3^{\text{visc,ve}}$	0.0824 (+2.0%)
	Case 3	$\hat{\varepsilon}$	0.0887
		$\hat{E}_1^{\text{visc,ve}}$	0.0874 (+1.5%)
		$\hat{E}_2^{\text{visc,ve}}$	0.0874 (+1.5%)
		$\hat{E}_3^{\text{visc,ve}}$	0.0874 (+1.5%)
		$\hat{E}_4^{\text{visc,ve}}$	0.0872 (+1.7%)
		$\hat{E}_5^{\text{visc,ve}}$	0.0872 (+1.8%)
PMMA/IM800A/PC	Case 1	$\hat{\varepsilon}$	0.161
		$\hat{E}_1^{\text{visc,ve}}$	0.152 (+5.9%)
	Case 2	$\hat{\varepsilon}$	0.144
		$\hat{E}_1^{\text{visc,ve}}$	0.136 (+5.9%)
		$\hat{E}_2^{\text{visc,ve}}$	0.136 (+6.0%)
	Case 3	$\hat{\varepsilon}$	0.138
		$\hat{E}_1^{\text{visc,ve}}$	0.139 (−0.4%)
		$\hat{E}_2^{\text{visc,ve}}$	0.139 (−0.4%)
		$\hat{E}_3^{\text{visc,ve}}$	0.139 (−0.3%)

strain tensor. In this approximation, the energy dissipated per unit volume by the mth term of the Prony series, $E_m^{\text{visc,ve}}$, is given by

$$E_m^{\text{visc,ve}} = \int_t \left[\frac{\beta_m}{2G_m} 2G_m \boldsymbol{\varepsilon}^{\text{dev}} : 2G_m \boldsymbol{\varepsilon}^{\text{dev}}\right] dt = 2G_m\beta_m \int_t \boldsymbol{\varepsilon}^{\text{dev}} : \boldsymbol{\varepsilon}^{\text{dev}} dt$$
$$= 3G_m\beta_m \int_t \bar{\varepsilon}^2 dt \tag{30}$$

where $\bar{\varepsilon} = \sqrt{\frac{2}{3}\boldsymbol{\varepsilon}^{\text{dev}} : \boldsymbol{\varepsilon}^{\text{dev}}}$ is the effective strain.

To ensure that Eq. (30) gives reasonably good estimate of the energy dissipated due to viscous effects, we compare at the final time of impact simulation the normalized total dissipation

$$\hat{E}_m^{\text{vise,ve}} = \sqrt{\frac{1}{3V_0 t_f G_m \beta_m} \int_{V_0} \left[E_m^{\text{vise,ve}}\Big|_{t=t_f} \right] dV_0} \tag{31}$$

obtained by using the actual dissipation calculated during the simulation, and its approximation

$$\hat{\varepsilon} = \sqrt{\frac{1}{V_0 t_f} \int_{V_0} \left[\int_{t=0}^{t_f} \bar{\varepsilon}^2 dt \right] dV_0} \tag{32}$$

calculated during the postprocessing of results. The values given in Table 8 clearly indicate that the approximate expression listed in Eq. (32) gives a very good estimate of the energy dissipated due to viscous effects. Moreover, one can see that the average strain $\hat{\varepsilon}$ is essentially the same for the three sets of values of material parameters.

We now use the approximate expression of Eq. (30) to explain that the viscous dissipation can decrease even if the viscoelastic contribution to the response of the material increases. Since values of $\hat{\varepsilon}$ given in Table 8 are virtually independent of the choice of the set of material parameters, the term $\int_t \bar{\varepsilon}^2 dt$ in Eq. (30) is the same for cases 1, 2, and 3 at the corresponding locations in the PMMA, the adhesive, and the PC and times. Rewriting Eq. (30) as

$$E^{\text{visc,ve}} = \sum_{m=1}^{M} \left[3G_m\beta_m \int_t \bar{\varepsilon}^2 dt \right] = \int_t \bar{\varepsilon}^2 dt \sum_{m=1}^{M} [3G_m\beta_m] \tag{33}$$

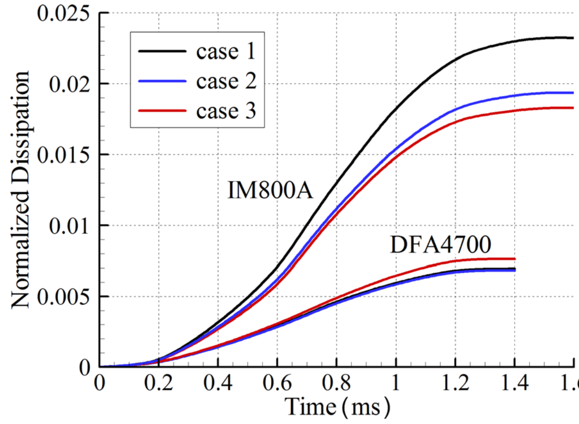

Fig. 20 For values of material parameters corresponding to cases 1, 2, and 3, the normalized total energy $\tilde{E}^{\text{vise.ve}}$ due to viscous deformations as function of time for the impact of PMMA/adhesive/PC plates with either DFA4700 or IM800A as adhesive

we see that the term $E^{\text{visc,ve}} / \sum_{m=1}^{M} 3G_m\beta_m$ is nearly the same for the three data sets. This is confirmed by the total normalized viscous dissipation $\tilde{E}^{\text{visc,ve}} = \left[\int_{V_0} E^{\text{visc,ve}} dV_0\right] \Big/ \left[t_f V_0 \sum_{m=21}^{M} 3G_m\beta_m\right]$ (we added the $t_f V_0$ term to obtain a dimensionless number) plotted in Fig. 20.

The curves in Fig. 20 are close to each other for the DFA4700 while for the IM800A the black curve is quantitatively different from the other two (20% difference at the final time). It follows from Eq. (30) that the energy dissipated due to viscous effects is proportional to $\sum_{m=1}^{M} G_m\beta_m$. Thus, even though $\sum_{m=1}^{M} G_m$ is larger in case 3 as compared to that in the other two cases, it does not imply that $\sum_{m=1}^{M} G_m\beta_m$ is also larger. The decrease in the relaxation times β_m's is so large that it more than compensates for the increase in the value of G_m's and the energy dissipated decreases. This explains why the IM800A with the set of material parameters for case 3 has less energy dissipated due to viscous deformations than that for values of material parameters for case 1. While the total viscoelastic contribution to the response is more important in case 3 the reduction by several orders of magnitude of some decay constants β_m results in a decrease in the energy dissipated. We note that the curves corresponding to the DFA4700 adhesive are below those corresponding to the IM800A adhesive which is related to the higher stiffness of the DFA4700 material and the consequent lower strains.

Conclusions

We have considered a simple constitutive equation for finite deformations of viscoelastic adhesives. For uniaxial tensile and compressive deformations at constant engineering axial strain rates, equations for the true axial stress have been derived as functions of the axial stretch and the axial stretch rate. Experimental data for uniaxial tests performed at constant engineering strain rates have been used to find values of material parameters for two adhesives, the DFA4700 and the more compliant IM800A. It is shown that depending upon the data used for monotonic loading, one cycle of loading and unloading, and two cycles of loading and unloading, values of material parameters are quite different. The tangent modulus at given values of the axial stretch and the axial stretch rate depends upon the data used to find values of material parameters. Thus, even for uniaxial deformations, one cannot correctly predict the experimental data not included in finding optimal values of the material parameters, and that improving the agreement with the first complete deformation cycle does not imply that the agreement with the second cycle is also improved.

The validity of the constitutive relations for three-dimensional deformations of the adhesive cannot be ascertained due to the nonexistence of the test data in the open literature. Values of the tangent modulus in simple shear deformations have been plotted as functions of the shear strain and the shear strain rate.

The constitutive equation has been implemented in the commercial FE software LS-DYNA and used to analyze transient deformations of a laminated plate impacted at low velocity by a rigid hemispherical nosed impactor. We found that the energy dissipated by viscous deformations of the adhesive interlayers decreased when more deformation cycles were included to find values of material parameters for the adhesive materials. However, the energy dissipated due to viscous deformations of the adhesive is miniscule relative to the kinetic energy of the impactor and the energy dissipated due to plastic deformations of the PC layer and cracking of the PMMA layer. Furthermore, it is found that plastic deformations of the PC layer, the fracture of the PMMA layer and the total energy dissipated are not sensitive to the values of material parameters used for the interlayer for the impact problem studied. This is due to the fact that using larger set of test data for finding values of the material parameters for the adhesive significantly affected their predicted low strain-rate response without impacting much their high strain-rate response.

Acknowledgment

This research was sponsored by the Army Research Laboratory and was accomplished under Cooperative Agreement No. W911NF-06-2-0014. The views and conclusions contained in this document are those of the authors and should not be interpreted as representing the official policies, either expressed or implied, of the Army Research Laboratory or the U.S. Government. The U.S. Government is authorized to reproduce and distribute reprints for government purposes notwithstanding any copyright notation hereon.

Appendix

Constitutive Relation for Viscoelastic Materials. We assume that the deformation gradient $\mathbf{F}$ and the strain-rate tensor $\mathbf{D}$ are given with respect to the global rectangular Cartesian coordinate axes.

In order to determine the contribution $\boldsymbol{\sigma}^{\text{nlel}}$ to the total Cauchy stress tensor $\boldsymbol{\sigma}$ we first find the eigensystem (i.e., eigenvectors $\{\mathbf{b}_i\}_{i=1,2,3}$ and eigenvalues $\{\eta_i\}_{i=1,2,3}$) of the left Cauchy–Green tensor $\mathbf{B}$:

$$\mathbf{B} = \mathbf{F}\cdot\mathbf{F}^{\mathrm{T}} = \sum_{i=1}^{3} \eta_i |\mathbf{b}_i\rangle\langle\mathbf{b}_i| \tag{A1}$$

where $|\mathbf{b}_i\rangle\langle\mathbf{b}_j|$ denotes the tensor product between vectors $\mathbf{b}_i$ and $\mathbf{b}_j$. The principal stretches $\{\lambda_i\}_{i=1,2,3}$ are related to the eigenvalues $\{\eta_i\}_{i=1,2,3}$ by $\lambda_i = \sqrt{\eta_i}$, $i = 1, 2, 3$. The Cauchy stress for the nonlinear elastic deformations can thus be written as [22]

$$\begin{aligned}\boldsymbol{\sigma}^{\text{nlel}} &= \frac{1}{J}\sum_{i=1}^{3}\lambda_i \frac{\partial W}{\partial \lambda_i}|\mathbf{b}_i\rangle\langle\mathbf{b}_i| \\ &= \frac{1}{\lambda_1\lambda_2\lambda_3}\sum_{i=1}^{3}\sum_{n=1}^{N}\mu\left[\tilde{\lambda}_i^{\alpha_n} - \frac{1}{3}\left(\tilde{\lambda}_1^{\alpha_n}+\tilde{\lambda}_2^{\alpha_n}+\tilde{\lambda}_3^{\alpha_n}\right)\right]|\mathbf{b}_i\rangle\langle\mathbf{b}_i|\end{aligned} \tag{A2}$$

where $\tilde{\lambda}_i = \lambda_i/(\lambda_1\lambda_2\lambda_3)^{1/3}$.

The Green–Naghdi stress rate requires that the rotation matrix $\mathbf{R}$ in the polar decomposition of the deformation gradient $\mathbf{F}$ be known. It is found from the relation

$$\mathbf{R} = \left(\sum_{i=1}^{3}\frac{1}{\lambda_i}|\mathbf{b}_i\rangle\langle\mathbf{b}_i|\right)\cdot\mathbf{F} \tag{A3}$$

Thus, the constitutive relation (5) for the viscoelastic contribution can be written as

$$\frac{d}{dt}\left[\mathbf{R}^{\mathrm{T}}\cdot\boldsymbol{\sigma}_m^{\text{ve}}\cdot\mathbf{R}\right] = 2G_m\mathbf{R}^{\mathrm{T}}\cdot\mathbf{D}^{\text{dev}}\cdot\mathbf{R} - \beta_m\mathbf{R}^{\mathrm{T}}\cdot\boldsymbol{\sigma}_m^{\text{ve}}\cdot\mathbf{R} \tag{A4}$$

Introducing $\hat{\boldsymbol{\sigma}}_m^{\text{ve}} = \mathbf{R}^{\mathrm{T}}\cdot\boldsymbol{\sigma}_m^{\text{ve}}\cdot\mathbf{R}$ and $\hat{\mathbf{D}}^{\text{dev}} = \mathbf{R}^{\mathrm{T}}\cdot\mathbf{D}^{\text{dev}}\cdot\mathbf{R}$, the contribution of the mth term of the Prony series $\boldsymbol{\sigma}_m^{\text{ve}}$ to the total Cauchy stress tensor can be incrementally updated according to

$$\begin{aligned}\boldsymbol{\sigma}_m^{\text{ve}}|_{t+\Delta t} &= (\mathbf{R}|_{t+\Delta t})\cdot(\hat{\boldsymbol{\sigma}}_m^{\text{ve}}|_{t+\Delta t})\cdot(\mathbf{R}|_{t+\Delta t})^{\mathrm{T}}, \\ \hat{\boldsymbol{\sigma}}_m^{\text{ve}}|_{t+\Delta t} &= \hat{\boldsymbol{\sigma}}_m^{\text{ve}}|_t + \left(2G_m\left(\hat{\mathbf{D}}^{\text{dev}}|_{t+\Delta t}\right) - \beta_m\left(\hat{\boldsymbol{\sigma}}_m^{\text{ve}}|_t\right)\right)\Delta t\end{aligned} \tag{A5}$$

In order to find the pressure for an incompressible material, the volume change is penalized by adding a contribution derived from the strain energy density function $W^{\text{vol}} = K(J - 1 - \ln(J))$ which results in adding the contribution $\boldsymbol{\sigma}^{\text{vol}}$ to the total Cauchy stress of the material where

$$\boldsymbol{\sigma}^{\text{vol}} = K\left(1-\frac{1}{J}\right)\mathbf{I} = K\left(1-\frac{1}{\lambda_1\lambda_2\lambda_3}\right)\mathbf{I} \tag{A6}$$

In Eq. (A6), $\mathbf{I}$ is the identity tensor, and the bulk modulus K is given by

$$K = \frac{2(1+\nu)}{3(1-2\nu)}\left[\frac{1}{2}\sum_{n=1}^{N}\mu_n\alpha_n + \sum_{m=1}^{M}G_m\right] \tag{A7}$$

where ν is Poisson's ratio of the material at zero strain.

Viscous Dissipation. We additively decompose the deviatoric strain-rate tensor into elastic and viscous parts

$$\mathbf{D}^{\text{dev}} = \mathbf{D}_m^{\text{el}} + \mathbf{D}_m^{\text{visc}} \tag{A8}$$

The constitutive relation (5) of the viscoelastic contribution can then be rewritten as

$$\overset{\bullet}{\boldsymbol{\sigma}}{}_m^{\text{ve}} = 2G_m\mathbf{D}^{\text{dev}} - \beta_m\boldsymbol{\sigma}_m^{\text{ve}} = 2G_m\left(\mathbf{D}^{\text{dev}} - \frac{\beta}{2G_m}\boldsymbol{\sigma}_m^{\text{ve}}\right) = 2G_m\mathbf{D}_m^{\text{el}} \tag{A9}$$

where we have set

$$\mathbf{D}_m^{\text{visc}} = \frac{\beta_m}{2G_m}\boldsymbol{\sigma}_m^{\text{ve}} \tag{A10}$$

which is valid for both incompressible and nearly incompressible materials. For an incompressible material, $\mathbf{D}^{\text{dev}} = \mathbf{D}$.

For an incompressible material, the rate of internal energy (work done to deform the material) per unit volume in the reference configuration equals $J\boldsymbol{\sigma}:\mathbf{D} = \boldsymbol{\sigma}:\mathbf{D}^{\text{dev}}$ and

$$\boldsymbol{\sigma}:\mathbf{D}^{\text{dev}} = \left(\boldsymbol{\sigma}^{\text{nlel}} + \sum_{m=1}^{M}\boldsymbol{\sigma}_m^{\text{ve}} - p\mathbf{I}\right):\mathbf{D}^{\text{dev}} \tag{A11a}$$

$$= \dot{W} + \sum_{m=1}^{m}\boldsymbol{\sigma}_m^{\text{ve}}:\mathbf{D}_m^{\text{el}} + \sum_{m=1}^{m}\boldsymbol{\sigma}_m^{\text{ve}}:\mathbf{D}_m^{\text{visc}} - p\,\mathrm{tr}\left(\mathbf{D}^{\text{dev}}\right) \tag{A11b}$$

Since $\mathrm{tr}\left(\mathbf{D}^{\text{dev}}\right) = 0$, Eq. (A11b) can be rewritten as

$$\boldsymbol{\sigma}:\mathbf{D}^{\text{dev}} = \dot{W} + \sum_{m=1}^{m}\boldsymbol{\sigma}_m^{\text{ve}}:\mathbf{D}_m^{\text{el}} + \sum_{m=1}^{m}\boldsymbol{\sigma}_m^{\text{ve}}:\mathbf{D}_m^{\text{visc}} \tag{A12a}$$

$$\boldsymbol{\sigma} : \mathbf{D}^{\text{dev}} = \dot{W} + \dot{E}^{\text{el,ve}} + \dot{E}^{\text{visc,ve}} \tag{A12b}$$

where $\dot{W}$ is the rate of energy of the nonlinear elastic contribution, $\dot{E}^{\text{el,ve}}$ is the rate of elastic energy of the viscoelastic contribution, and $\dot{E}^{\text{visc,ve}}$ is the rate of energy dissipated due to viscous deformations. We can use Eq. (A10) to obtain the following expression for the energy per unit volume dissipated due to viscous deformations:

$$E^{\text{visc,ve}} = \int_t \left[\sum_{m=1}^{M} \left(\frac{\beta_m}{2G_m} \boldsymbol{\sigma}_m^{\text{ve}} : \boldsymbol{\sigma}_m^{\text{ve}} \right) dt \right] \tag{A13}$$

Recalling Eqs. (1) and (5), we get

$$J\boldsymbol{\sigma} : \mathbf{D} = J\left(\boldsymbol{\sigma}^{\text{nlel}} + \boldsymbol{\sigma}^{\text{vol}} + \sum_{m=1}^{M} \boldsymbol{\sigma}_m^{\text{ve}} \right) : \mathbf{D} \tag{A14a}$$

$$= \dot{W} + \dot{W}^{\text{vol}} + J\sum_{m=1}^{M} \boldsymbol{\sigma}_m^{\text{ve}} : \mathbf{D}_m^{\text{el}} + J\sum_{m=1}^{M} \boldsymbol{\sigma}_m^{\text{ve}} : \mathbf{D}_m^{\text{visc}}$$
$$+ J\sum_{m=1}^{M} \boldsymbol{\sigma}_m^{\text{ve}} : \left(\mathbf{D} - \mathbf{D}^{\text{dev}} \right) \tag{A14b}$$

In order to prove that $\boldsymbol{\sigma}_m^{\text{ve}} : \left(\mathbf{D} - \mathbf{D}^{\text{dev}} \right) = 0$, we start with $\mathbf{D} - \mathbf{D}^{\text{dev}} = \frac{1}{3}\text{tr}(\mathbf{D})\mathbf{I}$ and simplify Eq. (A14*b*) by noticing that

$$\boldsymbol{\sigma}_m^{\text{ve}} : \left(\mathbf{D} - \mathbf{D}^{\text{dev}} \right) = \text{tr}\left(\boldsymbol{\sigma}_m^{\text{ve}} \cdot \frac{1}{3}\text{tr}(\mathbf{D})\mathbf{I} \right) = \frac{1}{3}\text{tr}\left(\boldsymbol{\sigma}_m^{\text{ve}}\right)\text{tr}(\mathbf{D}) \tag{A15}$$

We apply the trace operator to the constitutive relation (A9) which uses the Green–Naghdi stress-rate and obtain

$$\text{tr}\left(\mathbf{R} \cdot \frac{d}{dt}\left[\mathbf{R}^{\text{T}} \cdot \boldsymbol{\sigma}_m^{\text{ve}} \cdot \mathbf{R} \right] \cdot \mathbf{R}^{\text{T}} \right) = 2G_m \text{tr}\left(\mathbf{D}^{\text{dev}}\right) - \beta_m \text{tr}\left(\boldsymbol{\sigma}_m^{\text{ve}}\right) \tag{A16}$$

Equation (A16*b*) can be simplified and used with $\boldsymbol{\sigma}_m^{\text{ve}}|_{t=0} = 0$ to give the differential equation and the initial condition

$$\frac{d}{dt}\left[\text{tr}\left(\boldsymbol{\sigma}_m^{\text{ve}}\right) \right] = -\beta_m \text{tr}\left(\boldsymbol{\sigma}_m^{\text{ve}}\right), \quad \text{tr}\left(\boldsymbol{\sigma}_m^{\text{ve}}\right)|_{t=0} = 0 \tag{A17}$$

It follows from Eq. (A17) that $\text{tr}\left(\boldsymbol{\sigma}_m^{\text{ve}}\right) = 0$ at all times, which leads to the simplified expression:

$$J\boldsymbol{\sigma} : \mathbf{D} = \dot{W} + \dot{W}^{\text{vol}} + J\sum_{m=1}^{M} \boldsymbol{\sigma}_m^{\text{ve}} : \mathbf{D}_m^{\text{el}} + J\sum_{m=1}^{M} \boldsymbol{\sigma}_m^{\text{ve}} : \mathbf{D}_m^{\text{visc}} \tag{A18a}$$

$$= \dot{W} + \dot{W}^{\text{vol}} + \dot{E}^{\text{el,ve}} + \dot{E}^{\text{visc,ve}} \tag{A18b}$$

Here, $\dot{W}$ is the rate of elastic energy of the deviatoric nonlinear elastic contribution, $\dot{W}^{\text{vol}}$ is the rate of elastic energy due to the volumetric strain, $\dot{E}^{\text{el,ve}}$ is the rate of elastic energy of the viscoelastic contribution, and $\dot{E}^{\text{visc,ve}}$ is the rate of energy dissipated by viscous deformations. Using Eq. (A10), we get the following expression for the energy per unit undeformed volume dissipated due to viscous deformations:

$$E^{\text{visc,ve}} = \int_t \left[J\sum_{m=1}^{M} \left(\frac{\beta_m}{2G_m} \boldsymbol{\sigma}_m^{\text{ve}} : \boldsymbol{\sigma}_m^{\text{ve}} \right) dt \right] \tag{A19}$$

Stress–Strain Relations for Cyclic Tensile Tests. We recall the notations: $\mathbf{F}$ is the deformation gradient, λ is the axial stretch, λ_{T} is the transverse stretch, $\varepsilon^{\text{True}}$ is the true axial strain, ε^{Eng} is the engineering axial strain, $\dot{\varepsilon}^{\text{Eng}}$ is the engineering axial strain rate of the test, and $\lambda_{\text{I}}^{\text{p}}$, $\lambda_{\text{II}}^{\text{p}}$, $\lambda_{\text{III}}^{\text{p}}$, and $\lambda_{\text{IV}}^{\text{p}}$ are the peak axial stretches reached during cycles 1, 2, 3, and 4, respectively. We will use σ^{True} for the true (or Cauchy) axial stress and σ^{Eng} for the engineering axial stress

Constitutive Relations for Incompressible Material Under Uniaxial Loading. Since test data are available for large strains, we need to distinguish between engineering and true (or logarithmic) strains and strain rates. The engineering strain ε^{Eng} and the engineering stress σ^{Eng} are related to $\varepsilon^{\text{True}}$ and σ^{True} by

$$\varepsilon^{\text{True}} = \ln\left(1 + \varepsilon^{\text{Eng}}\right) = \ln(\lambda), \quad \sigma^{\text{True}} = \left(1 + \varepsilon^{\text{Eng}}\right)\sigma^{\text{Eng}} = \lambda\sigma^{\text{Eng}} \tag{A20}$$

With a proper choice of the coordinate system, we have

$$\mathbf{F} = \begin{pmatrix} \lambda & & \\ & \lambda_{\text{T}} & \\ & & \lambda_{\text{T}} \end{pmatrix} \tag{A21}$$

and since its determinant is one we have $\lambda_{\text{T}} = \lambda^{-1/2}$. It is clear from Eq. (A21) that the rotation matrix in the polar decomposition of $\mathbf{F}$ is the identity matrix at all times. Therefore, in the fixed frame of the experiment, the constitutive equations for the viscoelastic contribution can be simplified to give

$$\frac{d\boldsymbol{\sigma}_m^{\text{ve}}}{dt} = 2G_m\mathbf{D} - \beta_m\boldsymbol{\sigma}_m^{\text{ve}}, \quad \boldsymbol{\sigma}_m^{\text{ve}}|_{t=0} = 0 \tag{A22}$$

where we have used $\mathbf{D} = \mathbf{D}^{\text{dev}}$. The solution of Eq. (A22) is the convolution integral

$$\boldsymbol{\sigma}_m^{\text{ve}} = 2G_m \int_{\tau=0}^{t} e^{-\beta_m(t-\tau)}\mathbf{D}(\tau)d\tau \tag{A23}$$

where the strain-rate tensor $\mathbf{D}$ is given by

$$\mathbf{D} = \frac{1}{2}\left(\dot{\mathbf{F}}\mathbf{F}^{-1} + \mathbf{F}^{-\text{T}}\dot{\mathbf{F}}^{\text{T}} \right) = \frac{\dot{\lambda}}{\lambda}\begin{pmatrix} 1 & & \\ & -1/2 & \\ & & -1/2 \end{pmatrix} \tag{A24}$$

The quasi-static or elastic contribution to the material response is

$$\boldsymbol{\sigma}^{\text{nlel}} = \sum_{n=1}^{N} \mu_n \begin{pmatrix} \lambda^{\alpha_n} & & \\ & \lambda_{\text{T}}^{\alpha_n} & \\ & & \lambda_{\text{T}}^{\alpha_n} \end{pmatrix}$$
$$= \sum_{n=1}^{N} \mu_n \begin{pmatrix} \lambda^{\alpha_n} & & \\ & \lambda^{-\alpha_n/2} & \\ & & \lambda^{-\alpha_n/2} \end{pmatrix} \tag{A25}$$

Using Eqs. (A23) and (A25), we obtain the stress–strain relation

$$\boldsymbol{\sigma} = -p\mathbf{I} + \sum_{n=1}^{N} \mu_n \begin{pmatrix} \lambda^{\alpha_n} & & \\ & \lambda^{-\alpha_n/2} & \\ & & \lambda^{-\alpha_n/2} \end{pmatrix}$$
$$+ \left[\sum_{m=1}^{M} 2G_m \int_{\tau=0}^{t} e^{-\beta_m(t-\tau)} \left.\frac{\dot{\lambda}}{\lambda}\right|_{\tau} d\tau \right] \begin{pmatrix} 1 & & \\ & -1/2 & \\ & & -1/2 \end{pmatrix} \tag{A26}$$

To find the pressure p, we use the condition that the lateral faces of the body are traction-free, i.e., $\sigma_{22}(=\sigma_{33}) = 0$, and, therefore,

$$p = \sum_{n=1}^{N} \mu_n \lambda^{-\alpha_n/2} - \sum_{m=1}^{M} G_m \int_{\tau=0}^{t} e^{-\beta_m(t-\tau)} \left.\frac{\dot{\lambda}}{\lambda}\right|_{\tau} d\tau \tag{A27}$$

Thus, the axial stress $\sigma^{\rm True} = \sigma_{11}$ is given by

$$\sigma^{\rm True} = \sum_{n=1}^{N} \mu_n\left(\lambda^{\alpha_n} - \lambda^{-\alpha_n/2}\right) + \sum_{m=1}^{M} 3G_m \int_{\tau=0}^{t} e^{-\beta_m(t-\tau)} \left.\frac{\dot{\lambda}}{\lambda}\right|_{\tau} d\tau \tag{A28}$$

Cauchy Stress as Function of Axial Stretch for Deformations at Constant Engineering Strain Rate. We use here the convention that $\dot{\varepsilon}^{\rm Eng}$ is positive for the cyclic tensile tests in both loading and unloading. It represents the global engineering strain rate of the test and not the actual strain rate at which the material deforms. For the uniaxial compression test, $\dot{\varepsilon}^{\rm Eng}$ is negative. We will now give recursive relations that can be used to find the axial stress–axial stretch relations for an arbitrary number of cycles.

We introduce the exponential integral function Ei defined by $\mathrm{Ei} = -\int_{\xi=-x}^{+\infty}\left(e^{-\xi}/\xi d\xi\right)$ where the integral is understood as the Cauchy principal value due to the singularity of the integrand at 0.

- First cycle, loading

During the loading part of the first cycle, we have $\dot{\lambda} = \dot{\varepsilon}^{\rm Eng}$ (constant), and $\lambda = 1 + t\dot{\varepsilon}^{\rm Eng}$. Thus, the convolution integral in Eq. (A28) can be simplified to

$$\sigma^{\rm True}_{\rm I,load}(\lambda) = \sum_{n=1}^{N} \mu_n\left(\lambda^{\alpha_n} - \lambda^{-\alpha_n/2}\right) + \sum_{m=1}^{M} 3G_m \int_{\tau=0}^{t} e^{-\beta_m(t-\tau)} \frac{\dot{\varepsilon}^{\rm Eng}}{1+\tau\dot{\varepsilon}^{\rm Eng}} d\tau \tag{A29}$$

The time and the axial stretch are related by $t = (\lambda-1)/\dot{\varepsilon}^{\rm Eng}$, and we introduce for later use the function

$$\mathrm{I}_{\rm load}\left(\dot{\varepsilon}^{\rm Eng}, G, \beta, \lambda\right) = 3G\int_{\tau=0}^{(\lambda-1)/\dot{\varepsilon}^{\rm Eng}} \exp\left(-\beta\left(\frac{\lambda-1}{\dot{\varepsilon}^{\rm Eng}} - \tau\right)\right)\frac{\dot{\varepsilon}^{\rm Eng}}{1+\tau\dot{\varepsilon}^{\rm Eng}} d\tau \tag{A30a}$$

$$= 3G\exp\left(-\frac{\beta\lambda}{\dot{\varepsilon}^{\rm Eng}}\right)\left[\mathrm{Ei}\left(\frac{\beta\lambda}{\dot{\varepsilon}^{\rm Eng}}\right) - \mathrm{Ei}\left(\frac{\beta}{\dot{\varepsilon}^{\rm Eng}}\right)\right] \tag{A30b}$$

Thus, the axial stress as a function of the axial stretch is given by

$$\sigma^{\rm True}_{\rm I,load}(\lambda) = \sum_{n=1}^{N} \mu_n\left(\lambda^{\alpha_n} - \lambda^{-\alpha_n/2}\right) + \sum_{m=1}^{M} \mathrm{I}_{\rm load}\left(\dot{\varepsilon}^{\rm Eng}, G_m, \beta_m, \lambda\right) \tag{A31a}$$

$$= \sum_{n=1}^{N} \mu_n\left(\lambda^{\alpha_n} - \lambda^{-\alpha_n/2}\right) + \sum_{m=1}^{M} 3G_m \exp\left(-\frac{\beta_m\lambda}{\dot{\varepsilon}^{\rm Eng}}\right)\left[\mathrm{Ei}\left(\frac{\beta_m\lambda}{\dot{\varepsilon}^{\rm Eng}}\right) - \mathrm{Ei}\left(\frac{\beta_m}{\dot{\varepsilon}^{\rm Eng}}\right)\right] \tag{A31b}$$

which does not explicitly depend upon time.

- First cycle, unloading

The end time of the loading phase of the first cycle is given by $t^{\rm p}_{\rm I} = (\lambda^{\rm p}_{\rm I} - 1)/\dot{\varepsilon}^{\rm Eng}$. To obtain the expression for the stress in the unloading phase, we first note that

$$\int_{\tau=0}^{t} e^{-\beta_m(t-\tau)}\left.\frac{\dot{\lambda}}{\lambda}\right|_{\tau} d\tau = \int_{\tau=0}^{t^{\rm p}_{\rm I}} e^{-\beta_m(t-\tau)}\left.\frac{\dot{\lambda}}{\lambda}\right|_{\tau} d\tau + \int_{\tau=t^{\rm p}_{\rm I}}^{t} e^{-\beta_m(t-\tau)}\left.\frac{\dot{\lambda}}{\lambda}\right|_{\tau} d\tau \tag{A32a}$$

$$= e^{-\beta_m\left(t-t^{\rm p}_{\rm I}\right)}\int_{\tau=0}^{t^{\rm p}_{\rm I}} e^{-\beta_m\left(t^{\rm p}_{\rm I}-\tau\right)}\left.\frac{\dot{\lambda}}{\lambda}\right|_{\tau} d\tau + \int_{\xi=0}^{t-t^{\rm p}_{\rm I}} e^{-\beta_m\left(\left(t-t^{\rm p}_{\rm I}\right)-\xi\right)}\left.\frac{\dot{\lambda}}{\lambda}\right|_{t^{P}_{\rm I}+\xi} d\tau \tag{A32b}$$

Between $t^{\rm p}_{\rm I}$ and t (unloading), we have $\dot{\lambda} = -\dot{\varepsilon}^{\rm Eng}$ and $\lambda = \lambda^{\rm p}_{\rm I} - (\xi - t^{\rm p}_{\rm I})\dot{\varepsilon}^{\rm Eng}$, which leads to

$$\int_{\xi=0}^{t-t^{\rm p}_{\rm I}} e^{-\beta_m\left(\left(t-t^{\rm p}_{\rm I}\right)-\xi\right)}\left.\frac{\dot{\lambda}}{\lambda}\right|_{t^{P}_{\rm I}+\xi} d\tau = \int_{\xi=0}^{t-t^{\rm p}_{\rm I}} e^{-\beta_m\left(\left(t-t^{\rm p}_{\rm I}\right)-\xi\right)}\frac{-\dot{\varepsilon}^{\rm Eng}}{\lambda^{\rm p}_{\rm I} - \xi\dot{\varepsilon}^{\rm Eng}} d\tau \tag{A33}$$

In terms of the function

$$\mathrm{I}_{\rm unload}\left(\dot{\varepsilon}^{\rm Eng}, G, \beta, \lambda_0, \lambda\right) = 3G\int_{\xi=0}^{(\lambda_0-\lambda)/\dot{\varepsilon}^{\rm Eng}} \exp\left(-\beta\left(\frac{\lambda_0-\lambda}{\dot{\varepsilon}^{\rm Eng}} - \xi\right)\right) \times \frac{-\dot{\varepsilon}^{\rm Eng}}{\lambda_0 - \xi\dot{\varepsilon}^{\rm Eng}} d\tau \tag{A34a}$$

$$= 3G\exp\left(\frac{\beta\lambda}{\dot{\varepsilon}^{\rm Eng}}\right)\left[\mathrm{Ei}\left(-\frac{\beta\lambda}{\dot{\varepsilon}^{\rm Eng}}\right) - \mathrm{Ei}\left(-\frac{\beta\lambda_0}{\dot{\varepsilon}^{\rm Eng}}\right)\right] \tag{A34b}$$

the stress as a function of the stretch for the unloading phase of the first cycle is given by

$$\sigma^{\rm True}_{\rm I,unload}(\lambda) = \sum_{n=1}^{N} \mu_n\left(\lambda^{\alpha_n} - \lambda^{-\alpha_n/2}\right) \tag{A35a}$$

$$+ \sum_{m=1}^{M} \exp\left(-\beta_m, \frac{\lambda^{\rm p}_{\rm I} - \lambda}{\dot{\varepsilon}^{\rm Eng}}\right)\mathrm{I}_{\rm load}\left(\dot{\varepsilon}^{\rm Eng}, G_m, \beta_m, \lambda^{\rm p}_{\rm I}\right) + \sum_{m=1}^{M} \mathrm{I}_{\rm unload}\left(\dot{\varepsilon}^{\rm Eng}, G_m, \beta_m, \lambda^{\rm p}_{\rm I}, \lambda\right) \tag{A35b}$$

Substitution for $\mathrm{I}_{\rm load}$ from Eq. (A30b) and for $\mathrm{I}_{\rm unload}$ from Eq. (A34b) into Eq. (A35b) gives

$$\begin{aligned}\sigma^{\rm True}_{\rm I,unload}(\lambda) = {} & \sum_{n=1}^{N} \mu_n\left(\lambda^{\alpha_n} - \lambda^{-\alpha_n/2}\right) \\ & + \sum_{m=1}^{M} 3G_m \exp\left(-\beta_m\frac{2\lambda^{\rm p}_{\rm I} - \lambda}{\dot{\varepsilon}^{\rm Eng}}\right)\left[\mathrm{Ei}\left(\frac{\beta_m\lambda^{\rm p}_{\rm I}}{\dot{\varepsilon}^{\rm Eng}}\right) - \mathrm{Ei}\left(\frac{\beta_m}{\dot{\varepsilon}^{\rm Eng}}\right)\right] \\ & + \sum_{m=1}^{M} 3G_m \exp\left(\frac{\beta_m\lambda}{\dot{\varepsilon}^{\rm Eng}}\right)\left[\mathrm{Ei}\left(-\frac{\beta_m\lambda}{\dot{\varepsilon}^{\rm Eng}}\right) - \mathrm{Ei}\left(-\frac{\beta_m\lambda^{\rm p}_{\rm I}}{\dot{\varepsilon}^{\rm Eng}}\right)\right]\end{aligned} \tag{A36}$$

where there is no explicit dependence upon the time.

- Results for other cycles

One can obtain expression for the axial stress–axial stretch during subsequent cycles by using the integral splitting method in Eqs. (A32a) and (A32b) and functions $\mathrm{I}_{\rm load}$ and $\mathrm{I}_{\rm unload}$. That is, the stress during a loading (or unloading) phase of a cycle is the sum of the viscoelastic stress derived for the first loading (or unloading) cycle and of the viscoelastic stress existing at the beginning of the current phase with an exponential decay. The following expressions give the axial true stress as a function of the axial stretch without explicit dependence upon time (the stretch is a function of time). In order to show how they can be derived their expressions have not been fully simplified

$$\sigma^{\mathrm{True}}_{\mathrm{II,load}}(\lambda) = \sum_{n=1}^{N} \mu_n \left(\lambda^{\alpha_n} - \lambda^{-\alpha_n/2}\right) + \sum_{m=1}^{M} \exp\left(-\beta_m \left(\frac{\lambda^{\mathrm{p}}_{\mathrm{I}} - 1}{\dot{\varepsilon}^{\mathrm{Eng}}} + \Delta t + \frac{\lambda - 1}{\dot{\varepsilon}^{\mathrm{Eng}}}\right)\right) \mathrm{I}_{\mathrm{load}}\left(\dot{\varepsilon}^{\mathrm{Eng}}, G_m, \beta_m, \lambda^{\mathrm{p}}_{\mathrm{I}}\right)$$
$$+ \sum_{m=1}^{M} \exp\left(-\beta_m \left(\Delta t + \frac{\lambda - 1}{\dot{\varepsilon}^{\mathrm{Eng}}}\right)\right) \mathrm{I}_{\mathrm{unload}}\left(\dot{\varepsilon}^{\mathrm{Eng}}, G_m, \beta_m, \lambda^{\mathrm{p}}_{\mathrm{I}}, 1\right) + \sum_{m=1}^{M} \mathrm{I}_{\mathrm{load}}\left(\dot{\varepsilon}^{\mathrm{Eng}}, G_m, \beta_m, \lambda\right) \tag{A37}$$

$$\sigma^{\mathrm{True}}_{\mathrm{II,unload}}(\lambda) = \sum_{n=1}^{N} \mu_n \left(\lambda^{\alpha_n} - \lambda^{-\alpha_n/2}\right) + \sum_{m=1}^{M} \exp\left(-\beta_m \left(\frac{\lambda^{\mathrm{p}}_{\mathrm{I}} - 1}{\dot{\varepsilon}^{\mathrm{Eng}}} + \Delta t + \frac{\lambda^{\mathrm{p}}_{\mathrm{II}} - 1}{\dot{\varepsilon}^{\mathrm{Eng}}} + \frac{\lambda^{\mathrm{p}}_{\mathrm{II}} - \lambda}{\dot{\varepsilon}^{\mathrm{Eng}}}\right)\right) \mathrm{I}_{\mathrm{load}}\left(\dot{\varepsilon}^{\mathrm{Eng}}, G_m, \beta_m, \lambda^{\mathrm{p}}_{\mathrm{I}}\right)$$
$$+ \sum_{m=1}^{M} \exp\left(-\beta_m \left(\Delta t + \frac{\lambda^{\mathrm{p}}_{\mathrm{II}} - 1}{\dot{\varepsilon}^{\mathrm{Eng}}} + \frac{\lambda^{\mathrm{p}}_{\mathrm{II}} - \lambda}{\dot{\varepsilon}^{\mathrm{Eng}}}\right)\right) \mathrm{I}_{\mathrm{unload}}\left(\dot{\varepsilon}^{\mathrm{Eng}}, G_m, \beta_m, \lambda^{\mathrm{p}}_{\mathrm{I}}, 1\right) + \sum_{m=1}^{M} \exp\left(-\beta_m \frac{\lambda^{\mathrm{p}}_{\mathrm{II}} - \lambda}{\dot{\varepsilon}^{\mathrm{Eng}}}\right) \mathrm{I}_{\mathrm{load}}\left(\dot{\varepsilon}^{\mathrm{Eng}}, G_m, \beta_m, \lambda^{\mathrm{p}}_{\mathrm{II}}\right)$$
$$+ \sum_{m=1}^{M} \mathrm{I}_{\mathrm{unload}}\left(\dot{\varepsilon}^{\mathrm{Eng}}, G_m, \beta_m, \lambda^{\mathrm{p}}_{\mathrm{II}}, \lambda\right) \tag{A38}$$

$$\sigma^{\mathrm{True}}_{\mathrm{III,load}}(\lambda) = \sum_{n=1}^{N} \mu_n \left(\lambda^{\alpha_n} - \lambda^{-\alpha_n/2}\right) + \sum_{m=1}^{M} \exp\left(-\beta_m \left(\frac{\lambda^{\mathrm{p}}_{\mathrm{I}} - 1}{\dot{\varepsilon}^{\mathrm{Eng}}} + \Delta t + 2\frac{\lambda^{\mathrm{p}}_{\mathrm{II}} - 1}{\dot{\varepsilon}^{\mathrm{Eng}}} + \Delta t + \frac{\lambda - 1}{\dot{\varepsilon}^{\mathrm{Eng}}}\right)\right) \mathrm{I}_{\mathrm{load}}\left(\dot{\varepsilon}^{\mathrm{Eng}}, G_m, \beta_m, \lambda^{\mathrm{p}}_{\mathrm{I}}\right)$$
$$+ \sum_{m=1}^{M} \exp\left(-\beta_m \left(\Delta t + 2\frac{\lambda^{\mathrm{p}}_{\mathrm{II}} - 1}{\dot{\varepsilon}^{\mathrm{Eng}}} + \Delta t + \frac{\lambda - 1}{\dot{\varepsilon}^{\mathrm{Eng}}}\right)\right) \mathrm{I}_{\mathrm{unload}}\left(\dot{\varepsilon}^{\mathrm{Eng}}, G_m, \beta_m, \lambda^{\mathrm{p}}_{\mathrm{I}}, 1\right) + \sum_{m=1}^{M} \exp\left(-\beta_m \left(\frac{\lambda^{\mathrm{p}}_{\mathrm{II}} - 1}{\dot{\varepsilon}^{\mathrm{Eng}}} + \Delta t + \frac{\lambda - 1}{\dot{\varepsilon}^{\mathrm{Eng}}}\right)\right)$$
$$\times \mathrm{I}_{\mathrm{load}}\left(\dot{\varepsilon}^{\mathrm{Eng}}, G_m, \beta_m, \lambda^{\mathrm{p}}_{\mathrm{II}}\right) + \sum_{m=1}^{M} \exp\left(-\beta_m \left(\Delta t + \frac{\lambda - 1}{\dot{\varepsilon}^{\mathrm{Eng}}}\right)\right) \mathrm{I}_{\mathrm{unload}}\left(\dot{\varepsilon}^{\mathrm{Eng}}, G_m, \beta_m, \lambda^{\mathrm{p}}_{\mathrm{II}}, \lambda^{\mathrm{p}}_{\mathrm{II}}\right) + \sum_{m=1}^{M} \mathrm{I}_{\mathrm{load}}\left(\dot{\varepsilon}^{\mathrm{Eng}}, G_m, \beta_m, \lambda\right) \tag{A39}$$

$$\sigma^{\mathrm{True}}_{\mathrm{III,unload}}(\lambda) = \sum_{n=1}^{N} \mu_n \left(\lambda^{\alpha_n} - \lambda^{-\alpha_n/2}\right)$$
$$+ \sum_{m=1}^{M} \left[\exp\left(-\beta_m \left(\frac{\lambda^{\mathrm{p}}_{\mathrm{I}} - 1}{\dot{\varepsilon}^{\mathrm{Eng}}} + \Delta t + 2\frac{\lambda^{\mathrm{p}}_{\mathrm{II}} - 1}{\dot{\varepsilon}^{\mathrm{Eng}}} + \Delta t + \frac{\lambda^{\mathrm{p}}_{\mathrm{III}} - 1}{\dot{\varepsilon}^{\mathrm{Eng}}} + \frac{\lambda^{\mathrm{p}}_{\mathrm{III}} - \lambda}{\dot{\varepsilon}^{\mathrm{Eng}}}\right)\right) \mathrm{I}_{\mathrm{load}}\left(\dot{\varepsilon}^{\mathrm{Eng}}, G_m, \beta_m, \lambda^{\mathrm{p}}_{\mathrm{I}}\right)\right]$$
$$+ \sum_{m=1}^{M} \left[\exp\left(-\beta_m \left(\Delta t + 2\frac{\lambda^{\mathrm{p}}_{\mathrm{II}} - 1}{\dot{\varepsilon}^{\mathrm{Eng}}} + \Delta t + \frac{\lambda^{\mathrm{p}}_{\mathrm{III}} - 1}{\dot{\varepsilon}^{\mathrm{Eng}}} + \frac{\lambda^{P}_{\mathrm{III}} - \lambda}{\dot{\varepsilon}^{\mathrm{Eng}}}\right)\right) \mathrm{I}_{\mathrm{unload}}\left(\dot{\varepsilon}^{\mathrm{Eng}}, G_m, \beta_m, \lambda^{\mathrm{p}}_{\mathrm{I}}, 1\right)\right]$$
$$+ \sum_{m=1}^{M} \exp\left(-\beta_m \left(\frac{\lambda^{\mathrm{p}}_{II} - 1}{\dot{\varepsilon}^{\mathrm{Eng}}} + \Delta t + \frac{\lambda^{\mathrm{p}}_{\mathrm{III}} - 1}{\dot{\varepsilon}^{\mathrm{Eng}}} + \frac{\lambda^{\mathrm{p}}_{\mathrm{III}} - \lambda}{\dot{\varepsilon}^{\mathrm{Eng}}}\right)\right) I_{\mathrm{load}}\left(\dot{\varepsilon}^{\mathrm{Eng}}, G_m, \beta_m, \lambda^{\mathrm{p}}_{\mathrm{II}}, \lambda^{\mathrm{p}}_{\mathrm{II}}\right)$$
$$+ \sum_{m=1}^{M} \exp\left(-\beta_m \left(\Delta t + \frac{\lambda^{\mathrm{p}}_{\mathrm{III}} - 1}{\dot{\varepsilon}^{\mathrm{Eng}}} + \frac{\lambda^{\mathrm{p}}_{\mathrm{III}} - \lambda}{\dot{\varepsilon}^{\mathrm{Eng}}}\right)\right) \mathrm{I}_{\mathrm{unload}}\left(\dot{\varepsilon}^{\mathrm{Eng}}, G_m, \beta_m, \lambda^{\mathrm{p}}_{\mathrm{II}}, \lambda^{\mathrm{p}}_{\mathrm{II}}\right)$$
$$+ \sum_{m=1}^{M} \exp\left(-\beta_m \frac{\lambda^{\mathrm{p}}_{\mathrm{III}} - \lambda}{\dot{\varepsilon}^{\mathrm{Eng}}}\right) \mathrm{I}_{\mathrm{load}}\left(\dot{\varepsilon}^{\mathrm{Eng}}, G_m, \beta_m, \lambda^{\mathrm{p}}_{\mathrm{II}}\right) + \sum_{m=1}^{M} \mathrm{I}_{\mathrm{unload}}\left(\dot{\varepsilon}^{\mathrm{Eng}}, G_m, \beta_m, \lambda^{\mathrm{p}}_{\mathrm{III}}, \lambda\right) \tag{A40}$$

$$\sigma^{\mathrm{True}}_{\mathrm{IV,load}}(\lambda) = \sum_{n=1}^{N} \mu_n \left(\lambda^{\alpha_n} - \lambda^{-\alpha_n/2}\right) + \sum_{m=1}^{M} \left[\exp\left(-\beta_m \left(\frac{\lambda^{\mathrm{p}}_{\mathrm{I}} - 1}{\dot{\varepsilon}^{\mathrm{Eng}}} + \Delta t + 2\frac{\lambda^{\mathrm{p}}_{\mathrm{II}} - 1}{\dot{\varepsilon}^{\mathrm{Eng}}} + \Delta t + 2\frac{\lambda^{\mathrm{p}}_{\mathrm{III}} - 1}{\dot{\varepsilon}^{\mathrm{Eng}}} + \Delta t + \frac{\lambda - 1}{\dot{\varepsilon}^{\mathrm{Eng}}}\right)\right) \mathrm{I}_{\mathrm{load}}\left(\dot{\varepsilon}^{\mathrm{Eng}}, G_m, \beta_m, \lambda^{\mathrm{p}}_{\mathrm{I}}\right)\right]$$
$$+ \sum_{m=1}^{M} \left[\exp\left(-\beta_m \left(\Delta t + 2\frac{\lambda^{\mathrm{p}}_{\mathrm{II}} - 1}{\dot{\varepsilon}^{\mathrm{Eng}}} + \Delta t + 2\frac{\lambda^{\mathrm{p}}_{\mathrm{III}} - 1}{\dot{\varepsilon}^{\mathrm{Eng}}} + \Delta t + \frac{\lambda - 1}{\dot{\varepsilon}^{\mathrm{Eng}}}\right)\right) \mathrm{I}_{\mathrm{unload}}\left(\dot{\varepsilon}^{\mathrm{Eng}}, G_m, \beta_m, \lambda^{\mathrm{p}}_{\mathrm{I}}, 1\right)\right]$$
$$+ \sum_{m=1}^{M} \left[\exp\left(-\beta_m \left(\frac{\lambda^{\mathrm{p}}_{\mathrm{II}} - 1}{\dot{\varepsilon}^{\mathrm{Eng}}} + \Delta t + 2\frac{\lambda^{\mathrm{p}}_{\mathrm{III}} - 1}{\dot{\varepsilon}^{\mathrm{Eng}}} + \Delta t + \frac{\lambda_{-}1}{\dot{\varepsilon}^{\mathrm{Eng}}}\right)\right) I_{\mathrm{load}}\left(\dot{\varepsilon}^{\mathrm{Eng}}, G_m, \beta_m, \lambda^{\mathrm{p}}_{\mathrm{II}}\right)\right]$$
$$+ \sum_{m=1}^{M} \exp\left(-\beta_m \left(\Delta t + 2\frac{\lambda^{\mathrm{p}}_{\mathrm{III}} - 1}{\dot{\varepsilon}^{\mathrm{Eng}}} + \Delta t + \frac{\lambda - 1}{\dot{\varepsilon}^{\mathrm{Eng}}}\right)\right) \mathrm{I}_{\mathrm{unload}}\left(\dot{\varepsilon}^{\mathrm{Eng}}, G_m, \beta_m, \lambda^{\mathrm{p}}_{\mathrm{II}}, \lambda^{\mathrm{p}}_{\mathrm{II}}\right)$$
$$+ \sum_{m=1}^{M} \exp\left(-\beta_m \left(\frac{\lambda^{\mathrm{p}}_{\mathrm{III}} - 1}{\dot{\varepsilon}^{\mathrm{Eng}}} + \Delta t + \frac{\lambda - 1}{\dot{\varepsilon}^{\mathrm{Eng}}}\right)\right) \mathrm{I}_{\mathrm{load}}\left(\dot{\varepsilon}^{\mathrm{Eng}}, G_m, \beta_m, \lambda^{\mathrm{p}}_{\mathrm{II}}\right)$$
$$+ \sum_{m=1}^{M} \exp\left(-\beta_m \left(\Delta t + \frac{\lambda - 1}{\dot{\varepsilon}^{\mathrm{Eng}}}\right)\right) \mathrm{I}_{\mathrm{unload}}\left(\dot{\varepsilon}^{\mathrm{Eng}}, G_m, \beta_m, \lambda^{\mathrm{p}}_{\mathrm{III}}, 1\right)$$
$$+ \sum_{m=1}^{M} \mathrm{I}_{\mathrm{load}}\left(\dot{\varepsilon}^{\mathrm{Eng}}, G_m, \beta_m, \lambda\right) \tag{A41}$$

$$
\begin{aligned}
\sigma^{\mathrm{True}}_{\mathrm{IV,unload}}(\lambda) &= \sum_{n=1}^{N}\mu_n\left(\lambda^{\alpha_n}-\lambda^{-\alpha_n/2}\right)\\
&+\sum_{m=1}^{M}\left[\exp\left(-\beta_m\left(\frac{\lambda^{\mathrm{p}}_{\mathrm{I}}-1}{\dot{\varepsilon}^{\mathrm{Eng}}}+\Delta t+2\frac{\lambda^{\mathrm{p}}_{\mathrm{II}}-1}{\dot{\varepsilon}^{\mathrm{Eng}}}+\Delta t+2\frac{\lambda^{\mathrm{p}}_{\mathrm{III}}-1}{\dot{\varepsilon}^{\mathrm{Eng}}}+\Delta t+\frac{\lambda^{\mathrm{p}}_{\mathrm{IV}}-1}{\dot{\varepsilon}^{\mathrm{Eng}}}+\frac{\lambda^{\mathrm{p}}_{\mathrm{IV}}-\lambda}{\dot{\varepsilon}^{\mathrm{Eng}}}\right)\right)\mathrm{I}_{\mathrm{load}}\left(\dot{\varepsilon}^{\mathrm{Eng}},G_m,\beta_m,\lambda^{\mathrm{p}}_{\mathrm{I}}\right)\right]\\
&+\sum_{m=1}^{M}\left[\exp\left(-\beta_m\left(\Delta t+2\frac{\lambda^{\mathrm{p}}_{\mathrm{II}}-1}{\dot{\varepsilon}^{\mathrm{Eng}}}+\Delta t+2\frac{\lambda^{\mathrm{p}}_{\mathrm{III}}-1}{\dot{\varepsilon}^{\mathrm{Eng}}}+\Delta t+\frac{\lambda^{\mathrm{p}}_{\mathrm{IV}}-1}{\dot{\varepsilon}^{\mathrm{Eng}}}+\frac{\lambda^{\mathrm{p}}_{\mathrm{IV}}-\lambda}{\dot{\varepsilon}^{\mathrm{Eng}}}\right)\right)\mathrm{I}_{\mathrm{unload}}\left(\dot{\varepsilon}^{\mathrm{Eng}},G_m,\beta_m,\lambda^{\mathrm{p}}_{\mathrm{I}},1\right)\right]\\
&+\sum_{m=1}^{M}\left[\exp\left(-\beta_m\left(\frac{\lambda^{\mathrm{p}}_{\mathrm{II}}-1}{\dot{\varepsilon}^{\mathrm{Eng}}}+\Delta t+2\frac{\lambda^{\mathrm{p}}_{\mathrm{III}}-1}{\dot{\varepsilon}^{\mathrm{Eng}}}+\Delta t+\frac{\lambda^{\mathrm{p}}_{\mathrm{IV}}-1}{\dot{\varepsilon}^{\mathrm{Eng}}}+\frac{\lambda^{\mathrm{p}}_{\mathrm{IV}}-\lambda}{\dot{\varepsilon}^{\mathrm{Eng}}}\right)\right)I_{\mathrm{load}}\left(\dot{\varepsilon}^{\mathrm{Eng}},G_m,\beta_m,\lambda^{\mathrm{p}}_{\mathrm{II}}\right)\right]\\
&+\sum_{m=1}^{M}\left[\exp\left(-\beta_m\left(\Delta t+2\frac{\lambda^{\mathrm{p}}_{\mathrm{III}}-1}{\dot{\varepsilon}^{\mathrm{Eng}}}+\Delta t+\frac{\lambda^{\mathrm{p}}_{\mathrm{IV}}-1}{\dot{\varepsilon}^{\mathrm{Eng}}}+\frac{\lambda^{\mathrm{p}}_{\mathrm{IV}}-\lambda}{\dot{\varepsilon}^{\mathrm{Eng}}}\right)\right)\mathrm{I}_{\mathrm{unload}}\left(\dot{\varepsilon}^{\mathrm{Eng}},G_m,\beta_m,\lambda^{\mathrm{p}}_{\mathrm{II}},\lambda^{\mathrm{p}}_{\mathrm{II}}\right)\right]\\
&+\sum_{m=1}^{M}\exp\left(-\beta_m\left(\frac{\lambda^{\mathrm{p}}_{\mathrm{III}}-1}{\dot{\varepsilon}^{\mathrm{Eng}}}+\Delta t+\frac{\lambda^{\mathrm{p}}_{\mathrm{IV}}-\lambda}{\dot{\varepsilon}^{\mathrm{Eng}}}+\frac{\lambda^{\mathrm{p}}_{\mathrm{IV}}-\lambda}{\dot{\varepsilon}^{\mathrm{Eng}}}\right)\right)\mathrm{I}_{\mathrm{load}}\left(\dot{\varepsilon}^{\mathrm{Eng}},G_m,\beta_m,\lambda^{\mathrm{p}}_{\mathrm{II}}\right)\\
&+\sum_{m=1}^{M}\exp\left(-\beta_m\left(\Delta t+\frac{\lambda^{\mathrm{p}}_{\mathrm{IV}}-\lambda}{\dot{\varepsilon}^{\mathrm{Eng}}}+\frac{\lambda^{\mathrm{p}}_{\mathrm{IV}}-\lambda}{\dot{\varepsilon}^{\mathrm{Eng}}}\right)\right)\mathrm{I}_{\mathrm{unload}}\left(\dot{\varepsilon}^{\mathrm{Eng}},G_m,\beta_m,\lambda^{\mathrm{p}}_{\mathrm{III}},1\right)\\
&+\sum_{m=1}^{M}\exp\left(-\beta_m\frac{\lambda^{\mathrm{p}}_{\mathrm{IV}}-\lambda}{\dot{\varepsilon}^{\mathrm{Eng}}}\right)\mathrm{I}_{\mathrm{load}}\left(\dot{\varepsilon}^{\mathrm{Eng}},G_m,\beta_m,\lambda^{\mathrm{p}}_{\mathrm{IV}}\right)\\
&+\sum_{m=1}^{M}\mathrm{I}_{\mathrm{unload}}\left(\dot{\varepsilon}^{\mathrm{Eng}},G_m,\beta_m,\lambda^{\mathrm{p}}_{\mathrm{IV}},\lambda\right)
\end{aligned}
\tag{A42}
$$

Stress–Strain Relations for Simple Shear. We consider the plane stress finite shear deformation at constant engineering shear strain rate of an incompressible material. The deformation field can be written

$$x = X + \gamma Y,\quad y = Y,\quad z = Z \tag{A43}$$

where (x, y, z) and (X, Y, Z) are coordinates of the points occupied by the same material particle in the current and the reference configurations, respectively. Here, γ is the engineering shear strain, and since $\dot{\gamma}$ is constant, $\gamma = \dot{\gamma}t$ (here t is the time and the deformation starts at $t = 0$). The deformation gradient $\mathbf{F}$ is given by

$$\mathbf{F} = \begin{pmatrix} 1 & \gamma & \\ & 1 & \\ & & 1 \end{pmatrix} \tag{A44}$$

We find the polar decomposition $\mathbf{F} = \mathbf{V}\cdot\mathbf{R}$ with $\mathbf{V}$ symmetric positive definite and $\mathbf{R}$ proper orthogonal matrices. We denote by $\{\mathbf{v}_1, \mathbf{v}_2, \mathbf{v}_3\}$ and $\{\lambda_1, \lambda_2, \lambda_3\}$, respectively, the normalized eigenvectors and the eigenvalues of $\mathbf{V}$. Their values are

$$\mathbf{v}_1 = \begin{pmatrix} 0 \\ 0 \\ 1 \end{pmatrix},\quad \mathbf{v}_2 = \frac{1}{\sqrt{2}\sqrt{4+\gamma^2-\gamma\sqrt{4+\gamma^2}}}\begin{pmatrix} \gamma-\sqrt{4+\gamma^2} \\ 2 \\ 0 \end{pmatrix},$$

$$\mathbf{v}_3 = \frac{1}{\sqrt{2}\sqrt{4+\gamma^2-\gamma\sqrt{4+\gamma^2}}}\begin{pmatrix} 2 \\ -\gamma+\sqrt{4+\gamma^2} \\ 0 \end{pmatrix} \tag{A45a}$$

$$\lambda_1 = 1,\ \ \lambda_2 = \frac{\sqrt{2+\gamma^2-\gamma\sqrt{4+\gamma^2}}}{\sqrt{2}},\ \ \lambda_3 = \frac{\sqrt{2+\gamma^2+\gamma\sqrt{4+\gamma^2}}}{\sqrt{2}} \tag{A45b}$$

and the rotation matrix $\mathbf{R}$ is given by

$$\mathbf{R} = \begin{pmatrix} \dfrac{2}{\sqrt{4+\gamma^2}} & \dfrac{\gamma}{\sqrt{4+\gamma^2}} & 0 \\ \dfrac{-\gamma}{\sqrt{4+\gamma^2}} & \dfrac{2}{\sqrt{4+\gamma^2}} & 0 \\ 0 & 0 & 1 \end{pmatrix} \tag{A46}$$

The Cauchy stress corresponding to the nonlinear elastic contribution is

$$\boldsymbol{\sigma}^{\mathrm{Ogden}} = \sum_{n=1}^{N}\left[\mu_n\sum_{i=1}^{3}\lambda_i^{\alpha_n}|\mathbf{v}_i\rangle\langle\mathbf{v}_i|\right] \tag{A47}$$

To find the viscoelastic contribution we recall that the strain-rate tensor is the symmetric part of the velocity gradient $\mathbf{L} = \dot{\mathbf{F}}\cdot\mathbf{F}^{-1}$, and after defining the corotated quantities $\hat{\boldsymbol{\sigma}}^{\mathrm{ve}}_m = \mathbf{R}^{\mathrm{T}}\cdot\boldsymbol{\sigma}^{\mathrm{ve}}_m\cdot\mathbf{R}$ and $\hat{\mathbf{D}} = \mathbf{R}^{\mathrm{T}}\cdot\mathbf{D}\cdot\mathbf{R}$ (see Eq. (A4)) the contribution of the mth term of the Prony series to the viscoelastic response of the material is given by

$$\frac{d}{dt}\left(\hat{\boldsymbol{\sigma}}^{\mathrm{ve}}_m\right) = 2G_m\hat{\mathbf{D}} - \beta_m\hat{\boldsymbol{\sigma}}^{\mathrm{ve}}_m = G_m\mathbf{R}^{\mathrm{T}}\cdot\begin{pmatrix} 0 & \dot{\gamma} & \\ \dot{\gamma} & 0 & \\ & & 0 \end{pmatrix}\cdot\mathbf{R} - \beta_m\hat{\boldsymbol{\sigma}}^{\mathrm{ve}}_m \tag{A48}$$

With the condition $\hat{\boldsymbol{\sigma}}^{\mathrm{ve}}_m\big|_{t=0} = \mathbf{0}$ the differential equation (A48) is numerically solved for the six independent components of the symmetric tensor $\hat{\boldsymbol{\sigma}}^{\mathrm{ve}}_m$ using the "NDSolve" function of MATHEMATICA. Thus, $\boldsymbol{\sigma}^{\mathrm{ve}}_m = \mathbf{R}\cdot\hat{\boldsymbol{\sigma}}^{\mathrm{ve}}_m\cdot\mathbf{R}^{\mathrm{T}}$.

We find the hydrostatic pressure from the condition $\sigma_{zz} = -p + \sum_{n=1}^{N}\mu_n + \sum_{m=1}^{M}\left(\boldsymbol{\sigma}^{\mathrm{ve}}_m\right)_{zz} = 0$. We note that due to the structure of the rotation matrix $\mathbf{R}$ the differential equation for $\left(\boldsymbol{\sigma}^{\mathrm{ve}}_m\right)_{zz}$ is uncoupled from the differential equations for the remaining components, and we get $\left(\boldsymbol{\sigma}^{\mathrm{ve}}_m\right)_{zz} = 0$ identically.

The (engineering) shear stress σ_{xy} can be computed from Eq. (A47) and from the numerical solution of Eq. (A48). The tangent shear modulus is then defined as $G_T = \partial\sigma_{xy}/\partial\gamma$ and is numerically evaluated.

References

[1] Hepburn, C., 1982, *Polyurethane Elastomers*, Applied Science Publishers, London, UK.

[2] Cooper, S. L., and Tobolsky, A. V., 1966, "Properties of Linear Elastomeric Polyurethanes," J. Appl. Polym. Sci., **10**(12), pp. 1837–1844.

[3] Sanchez-Adsuar, M. S., and Martin-Martinez, J. M., 2000, "Structure, Composition, and Adhesion Properties of Thermoplastic Polyurethane Adhesives," J. Adhes. Sci. Technol., **14**(8), pp. 1035–1055.

[4] Yi, J., Boyce, M. C., Lee, G. F., and Balizer, E., 2006, "Large Deformation Rate-Dependent Stress–Strain Behavior of Polyurea and Polyurethanes," Polymer, **47**(1), pp. 319–329.

[5] Petrovic, Z. S., and Ferguson, J., 1991, "Polyurethane Elastomers," Prog. Polym. Sci., **16**(5), pp. 695–836.
[6] Budinski, K. G., and Budinski, M. K., 2009, *Engineering Materials: Properties and Selection*, 9th ed., Prentice-Hall, Upper Saddle River, NJ.
[7] Tasdemirci, A., Hall, I. W., Gama, B. A., and Guiden, M., 2004, "Stress Wave Propagation Effects in Two- and Three-Layered Composite Materials," J. Compos. Mater., **38**(12), pp. 995–1009.
[8] Kihara, K., Isono, H., Yamabe, H., and Sugibayashi, T., 2003, "A Study and Evaluation of the Shear Strength of Adhesive Layers Subjected to Impact Loads," Int. J. Adhes. Adhes., **23**(4), pp. 253–259.
[9] Sarva, S. S., Deschanel, S., Boyce, M. C., and Chen, W. N., 2007, "Stress–Strain Behavior of a Polyurea and a Polyurethane From Low to High Strain Rates," Polymer, **48**(8), pp. 2208–2213.
[10] Rivlin, R., and Saunders, D., 1997, *Large Elastic Deformations of Isotropic Materials* (Collected Papers of R. S. Rivlin), Springer, New York, pp. 318–351.
[11] Ericksen, J. L., 1954, "Deformations Possible in Every Isotropic, Incompressible, Perfectly Elastic Body," Z. Angew. Math. Phys. (ZAMP), **5**(6), pp. 466–489.
[12] Ogden, R., 1972, "Large Deformation Isotropic Elasticity—On the Correlation of Theory and Experiment for Incompressible Rubberlike Solids," Proc. R. Soc. London, Ser. A, **326**(1567), pp. 565–584.
[13] Arruda, E. M., and Boyce, M. C., 1993, "A 3-Dimensional Constitutive Model for the Large Stretch Behavior of Rubber Elastic-Materials," J. Mech. Phys. Solids, **41**(2), pp. 389–412.
[14] Coleman, B. D., and Noll, W., 1961, "Foundations of Linear Viscoelasticity," Rev. Mod. Phys., **33**(2), pp. 239–249.
[15] Christensen, R. M., 1980, "A Non-Linear Theory of Viscoelasticity for Application to Elastomers," ASME J. Appl. Mech., **47**(4), pp. 762–768.
[16] Qi, H. J., and Boyce, M. C., 2005, "Stress–Strain Behavior of Thermoplastic Polyurethanes," Mech. Mater., **37**(8), pp. 817–839.
[17] Boyce, M. C., Kear, K., Socrate, S., and Shaw, K., 2001, "Deformation of Thermoplastic Vulcanizates," J. Mech. Phys. Solids, **49**(5), pp. 1073–1098.
[18] Boyce, M. C., Socrate, S., Kear, K., Yeh, O., and Shaw, K., 2001, "Micromechanisms of Deformation and Recovery in Thermoplastic Vulcanizates," J. Mech. Phys. Solids, **49**(6), pp. 1323–1342.
[19] Antoine, G. O., and Batra, R. C., 2014, "Low Speed Impact of Laminated Polymethylmethacrylate/Adhesive/Polycarbonate Plates," Compos. Struct., **116**, pp. 193–210.
[20] Ogden, R. W., 1997, *Non-Linear Elastic Deformations*, Courier Dover Publications, Mineola, NY.
[21] Green, A. E., and Naghdi, P. M., 1965, "A General Theory of an Elastic-Plastic Continuum," Arch. Ration. Mech. Anal., **18**(4), pp. 251–281.
[22] Batra, R. C., 2006, *Elements of Continuum Mechanics, Education Series*, American Institute of Aeronautics and Astronautics, Reston, VA.
[23] Stenzler, J. S., 2009, "Impact Mechanics of PMMA/PC Multi-Laminates With Soft Polymer Interlayers," M.Sc. thesis, Virginia Polytechnic Institute and State University, Blacksburg, VA.
[24] Bapat, C. N., and Batra, R. C., 1984, "Finite Plane-Strain Deformations of Nonlinear Viscoelastic Rubber-Covered Rolls," Int. J. Numer. Methods Eng., **20**(10), pp. 1911–1927.
[25] Batra, R. C., and Yu, J. H., 1999, "Linear Constitutive Relations in Isotropic Finite Viscoelasticity," J. Elast., **55**(1), pp. 73–77.
[26] Yu, J. H., and Batra, R. C., 2000, "Constrained Layer Damping in Finite Shearing Deformations," J. Sound Vib., **229**(2), pp. 445–452.
[27] Batra, R. C., and Yu, J. H., 2000, "Torsion of a Viscoelastic Cylinder," ASME J. Appl. Mech., **67**(2), pp. 424–427.
[28] Batra, R. C., and Kim, C. H., 1990, "Effect of Viscoplastic Flow Rules on the Initiation and Growth of Shear Bands at High-Strain Rates," J. Mech. Phys. Solids, **38**(6), pp. 859–874.
[29] Simo, J. C., and Taylor, R. L., 1982, "Penalty-Function Formulations for Incompressible Non-Linear Elastostatics," Comput. Methods Appl. Mech. Eng., **35**(1), pp. 107–118.
[30] Kröner, E., 1959, "Allgemeine Kontinuumstheorie Der Versetzungen Und Eigenspannungen," Arch. Ration. Mech. Anal., **4**(1), pp. 273–334.
[31] Lee, E. H., 1969, "Elastic–Plastic Deformation at Finite Strains," ASME J. Appl. Mech., **36**(1), pp. 1–6.